

NASA TECHNICAL NOTE



NASA TN D-4534

C.1



NASA TN D-4534

LOAN COPY: RETURN TO
AFWL (WLIL-2)
KIRTLAND AFB, N MEX

OPTIMAL FINITE-THRUST TRANSFER BETWEEN PLANET-APPROACH AND DEPARTURE ASYMPTOTES WITH SPECIFIED INTERMEDIATE ORBIT

by Edward A. Willis, Jr.

Lewis Research Center

Cleveland, Ohio





OPTIMAL FINITE-THRUST TRANSFER BETWEEN PLANET-APPROACH
AND DEPARTURE ASYMPTOTES WITH SPECIFIED
INTERMEDIATE ORBIT

By Edward A. Willis, Jr.

Lewis Research Center
Cleveland, Ohio

NATIONAL AERONAUTICS AND SPACE ADMINISTRATION

For sale by the Clearinghouse for Federal Scientific and Technical Information
Springfield, Virginia 22151 - CFSTI price \$3.00



ABSTRACT

Optimal-control and finite-thrust aspects of the approach maneuver - planetocentric orbit - departure maneuver sequence at the destination planet of a round trip are studied. Solutions are developed for single maneuvers, and conditions for joining these into an optimal total trajectory are derived. Numerical results are presented for an elliptic parking orbit and typical asymptotic velocities and directions. It is shown that "gravity losses" and "steering losses" are not directly additive, low vehicle thrust to weight ratios are desirable, and trajectories with single-burn escape and capture maneuvers are usually advantageous.

CONTENTS

	Page
SUMMARY	1
INTRODUCTION	2
SYMBOLS	4
ANALYSIS	7
Assumptions and Basic Equations	8
Equations of motion	9
Boundary conditions	11
Variational Necessary Conditions	13
Optimal control laws	14
Transversality conditions	15
Optimal Trajectory Solutions	16
Impulsive thrust	16
Mean value solution	20
Microthrust	21
Variational solutions for finite thrust	22
Near-optimal feedback solutions	23
Matching Conditions for Combined Maneuvers	23
RESULTS AND DISCUSSION.	25
Individual Escape or Capture Maneuvers.	27
Effect of asymptotic direction	27
Effect of asymptotic velocity	31
Characteristics of finite-thrust trajectories.	31
Combined Trajectories	33
Matching procedure.	33
Comparison of single- and multiple-burn maneuvers	35
Sample Application	37
CONCLUDING REMARKS	40
APPENDIXES	
A - SINGULAR ARCS AND PARAMETER OPTIMIZATION	42
B - PARTIAL DERIVATIVES FOR THE TRANSVERSALITY CONDITIONS	44
C - NEAR-OPTIMAL FEEDBACK SOLUTION	47
REFERENCES.	56

OPTIMAL FINITE-THRUST TRANSFER BETWEEN PLANET-APPROACH
AND DEPARTURE ASYMPTOTES WITH SPECIFIED
INTERMEDIATE ORBIT

by Edward A. Willis, Jr.

Lewis Research Center

SUMMARY

This report deals with finite-thrust and optimal-control aspects of the approach maneuver - planetocentric orbit - departure maneuver trajectory sequence at the destination of an interplanetary round trip. Individual escape or capture maneuvers (with constant, continuous acceleration) leading from an arbitrary planetocentric orbit to a specified hyperbolic asymptote are first studied using the Pontryagin maximum principle. An analytical "matching condition" is then derived which permits an optimal approach - orbit - departure trajectory sequence to be constructed from single maneuver data. Representative results obtained in this manner are compared with alternative (multiburn) solutions to this same problem. It is shown that the present "single-burn" class of solutions is usually superior unless the asymptotic direction constraint is very severe.

It is also found that "gravity losses" due to finite thrust and "steering losses" due to constraints on the asymptotic direction do not add together directly. In the medium to high acceleration regime, gravity losses occur primarily in connection with near-optimal-angle maneuvers (i. e., with no asymptotic constraints). When the asymptotic direction is strongly constrained, there are large steering losses but little or no additional penalty for finite thrust. It is concluded that the steering losses can be offset to a significant extent by using a relatively small, lightweight engine which need not develop vehicle accelerations larger than a few percent of local gravity. This is illustrated in terms of a specific mission (stopover round trip to Jupiter using nuclear rockets). For the case considered, it is found that the most desirable vehicle thrust to weight ratio at Jupiter is in the range of 0.01 to 0.03 local gravity (0.02 to 0.06 Earth gravity).

INTRODUCTION

Many significant problems remain before an ambitious interplanetary round trip like the one in figure 1(a) can be accomplished. Trajectory problems in particular require early attention because their solutions comprise an essential "input" for hardware-oriented studies such as the selection of a desirable engine type and size for future development. One of the most interesting parts of the total trajectory is the multipoint boundary value problem arising at the destination planet of a round trip. There the space vehicle must transfer between prescribed hyperbolic asymptotes by way of an intermediate parking orbit, as suggested by figure 1(b). The two asymptotes are defined at the

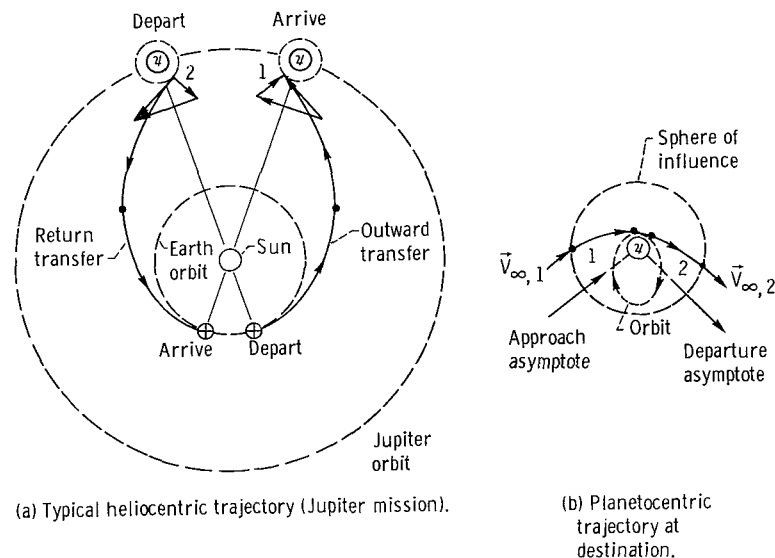
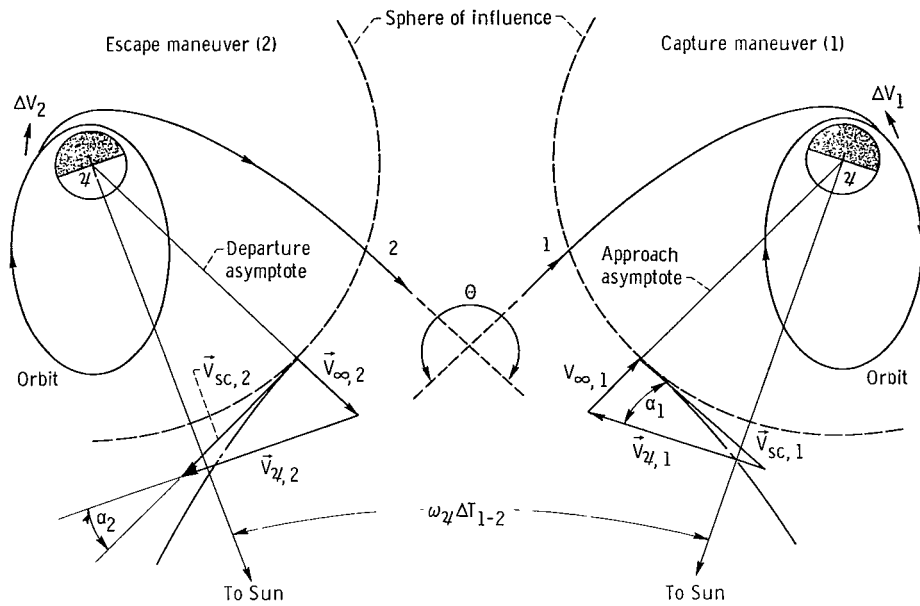


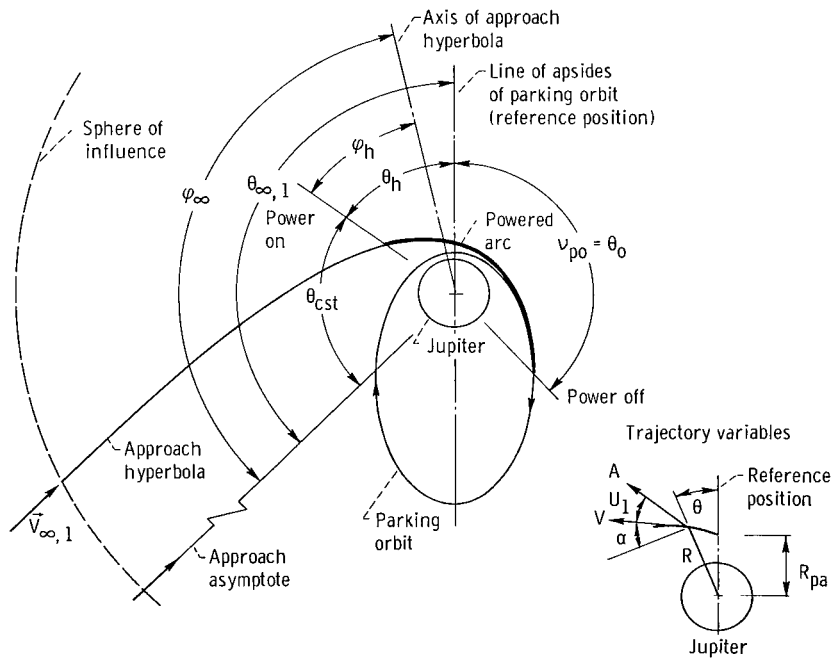
Figure 1. - Elements of interplanetary trajectories.

sphere of influence by the hyperbolic velocity vectors $\vec{V}_{\infty, 1}$ and $\vec{V}_{\infty, 2}$ as shown in figure 2(a). The intermediate orbit itself represents a third boundary condition which with one of the two asymptotes leads to the single-maneuver geometry illustrated in figure 2(b). The problem, then, is to accomplish the indicated approach maneuver - intermediate orbit - departure maneuver sequence with minimum propulsive effort or ΔV .

Solutions are easily obtained if the intermediate orbit is circular; the geometric boundary value aspect is then trivial, and the question of optimally escaping from a circular orbit has already been discussed at length (e.g., in refs. 1 to 4). But when an elliptic or hyperbolic orbit is used, the solutions are more interesting because several extra degrees of freedom are then relevant. Prior studies of the elliptic-parking-orbit case (refs. 5 to 7) consider only the impulsive thrust limit. These results (which are



(a) Derivation of boundary conditions.



(b) Finite-thrust capture maneuver.

Figure 2. - Geometry of planetocentric maneuvers.

applicable to stopover missions) indicate large ΔV reductions in particular examples for using an elliptic rather than a circular parking orbit. Even greater ΔV savings are obtained for nonstop round trips for which the intermediate orbit is hyperbolic. In this case also, prior studies such as references 8 and 9 are limited to the impulsive thrust approximation. These results are of undoubted value because in many cases they provide limits of performance and a qualitatively correct description of the problem. On the other hand, it is clear that more realistic methods are needed to support detailed mission studies which might involve, for example, the determination of optimal engine sizes or vehicle thrust to weight ratios.

Accordingly, the present analysis deals with finite-thrust and optimal-control aspects of the problem illustrated in figure 2. It is intended to be a direct extension of reference 4, which treated only the optimal-angle case for individual (escape or capture) maneuvers. The question of minimizing ΔV is approached by separating the total trajectory into a pair of escape and capture maneuvers (as shown in fig. 2(b)). These are studied individually using Pontryagin's maximum principle (ref. 10) and then assembled by means of a matching condition to produce an optimal overall solution.

For single-burn escape and capture maneuvers, the propulsive effort (ΔV) and the associated state and control variable histories are studied as functions of the magnitude and direction of \vec{V}_∞ . Limits of performance are defined in terms of closed-form variational solutions valid in the limits of impulsive or very low thrust. (The impulsive solution is also used as the basis of a stable and very efficient feedback algorithm; this furnishes a convenient means of approximating the variational results presented herein.)

A simple analytical matching condition is derived from the principle of "equal incremental slopes". This permits the angular constraint to be distributed optimally between the escape and capture arcs (without the need for trial-and-error searching) and thereby yields an optimal overall trajectory.

Illustrative numerical results are presented, and the global optimality of the present (single-burn) class of solutions is discussed by comparing them in an approximate manner with multiburn maneuvers which also yield low ΔV .

Finally, an example is given (stopover round trip to Jupiter) to illustrate how the present results may affect important questions such as the selection of an advantageous engine type and size for future development.

SYMBOLS

- A acceleration
- a dimensionless acceleration, see eq. (4)
- b auxiliary function used in appendixes A and C

D	defined in eq. (20)
E	terminal error function, see eq. (46)
$\mathcal{E}_1, \mathcal{E}_2, \mathcal{E}_3$	components of terminal error function, see eq. (46)
e	eccentricity of conic section
F	defined in eq. (11)
f_v	gravity and steering loss ΔV correction factor, $\Delta V/\Delta V_{\min}$
G	acceleration due to gravity
g	dimensionless acceleration due to gravity, see eq. (4)
H	angular momentum
\mathcal{H}	Hamiltonian function
h	angular momentum/ $R_{pa} V_{c, pa}$
I	specific impulse, sec
K	thrust switching function
M	mass
m	mass fraction
P	magnitude of primer vector, see eq. (16)
p	semilatus rectum/ R_{pa}
R	polar radius
r	dimensionless radius, see eq. (4)
T	orbital period
t	time
U_1	thrust angle of attack
U_2	thrust magnitude control function
V	velocity
ΔV	propulsive velocity increment
ΔV_{\min}	impulsive ΔV for unconstrained asymptotic direction, see eq. (32)
v	dimensionless velocity, see eq. (4)
Δv	propulsive velocity increment in dimensionless units, $\Delta V/V_{c, pa}$
X	correlation angle, defined by eq. (54)

Y	auxiliary function defined in eq. (C10)
α	trajectory path angle
η	efficiency
Θ	angle between hyperbolic asymptotes
θ	trajectory central angle measured from major axis of intermediate orbit
μ	planet gravitational constant
ν	parking orbit true anomaly at thrust initiation (escape maneuver) or at thrust termination (capture)
σ	mismatch angle, see p. 35
τ	dimensionless time, measured from zero at the inner end of a trajectory positively toward the sphere of influence
φ	true anomaly on escape or capture hyperbola
ψ_i	adjoint variables
ω	planet angular velocity, see fig. 2
$()'$	denotes differentiation with respect to τ
$\langle \rangle$	denotes mean value
$()^*$	denotes temporary normalization

Subscripts:

aa	apoapse
act	actual
c	circular
cst	coasting
des	desired
e	engine
g	to be gained
h	junction between powered arc and approach or departure hyperbola
i, j, k	general numerical indices
imp	impulsive
m	mean
max	maximum

min	minimum
o	junction between powered arc and planetocentric orbit
opt	optimal
p	propellant
pa	periapse
pl	planet
po	parking or intermediate orbit
pr	propulsive
ref	reference
sc	spacecraft
∞	sphere of influence
$\text{\textcircled{J}}$	Jupiter
$\text{\textcircled{\oplus}}$	Earth
1	capture maneuver at destination planet
2	escape maneuver at destination planet

ANALYSIS

The stated problem involves trajectories which are consistent with the boundary conditions illustrated in figure 2 and for which the sum of the capture and escape propulsive velocity increments

$$\Delta V_1 + \Delta V_2 \quad (1)$$

is a minimum. For example, the escape maneuver contributes an amount

$$\Delta V_2 = \int_{t_0}^{t_h} \frac{\text{Thrust}}{\text{Mass}} dt$$

to this criterion. This is directly related to space vehicle mass by the classical rocket equation which may be written as

$$M_{1,h} = M_{2,h} \exp\left(\frac{\Delta V_1 + \Delta V_2}{IG_{\oplus}}\right) \quad (2)$$

when the propulsion system operates with constant jet velocity (i. e., IG_{\oplus}) and no mass is jettisoned between the escape and capture maneuvers. The approach used in minimizing equation (1) is, first, to study individual maneuvers which yield minimum ΔV for arbitrary magnitude and direction of \vec{V}_{∞} , and second, to develop matching conditions which, when satisfied jointly by the escape and capture maneuvers, will produce an optimal overall trajectory.

Assumptions and Basic Equations

The planetocentric orbit escape or capture maneuver as illustrated in figure 2(b) is studied under the following conventions:

(1) In keeping with the usual "successive two-body" trajectory model, an interplanetary trip (fig. 1) is viewed as consisting of alternate heliocentric and planetocentric arcs matched at the sphere of influence of each planet as indicated in figure 2(a). The radius of the sphere of influence is taken to be negligible in comparison with interplanetary distances yet very much larger than a characteristic dimension of the planetocentric orbit (for instance the apoapse of an ellipse). This further implies that only the magnitude and direction of \vec{V}_{∞} are specified. Its lateral displacement relative to planet center is taken as an open parameter for optimization.

(2) The only external forces along the trajectory are the engine thrust and inverse-square gravitational attraction.

(3) The entire planetocentric trajectory (fig. 1(b)) lies in a single plane passing through the center of force and containing the two asymptote vectors $\vec{V}_{\infty,1}$ and $\vec{V}_{\infty,2}$.

(4) The $\vec{V}_{\infty,1}$ and $\vec{V}_{\infty,2}$ vectors are regarded as being determined in magnitude and direction by prior heliocentric calculations such as those in reference 7. Thus, possible interactions between heliocentric and planetocentric trajectory optimizations are disregarded here.

(5) The previous four points further imply that the maneuver time (from initiation of the first burn until escape energy has been reached) must not exceed a small fraction of the time spent within the sphere of influence. If this were not so, then either the asymptotes derived from interplanetary calculations would be invalidated, or a significant part of the planetary stay time would be spent in accomplishing propulsive maneuvers instead of performing mission objectives.

(6) Primary attention is directed toward the class of single-burn maneuvers; these are deemed preferable because of their simplicity and their short maneuver times. Moreover, it will be demonstrated that they are usually superior to the multiburn solutions when both types are required to satisfy item (5). These single-burn trajectories consist of a continuous-thrust maneuver from the orbit departure point to burnout; a coasting arc then proceeds to the sphere of influence where it must yield the desired magnitude and direction of \vec{V}_∞ .

(7) Vehicle dynamics are neglected; it is assumed that commanded control settings are attained without significant lag.

(8) The continuously variable direction and bounded magnitude of the vehicle acceleration are taken as the primary control functions. Also to be optimized are the power-on and power-off points, the lateral displacements of the two \vec{V}_∞ vectors, and the orientation of the intermediate orbit relative to these vectors.

With a result anticipated, it will be shown that the assumption of bounded acceleration effectively eliminates the specific impulse I from consideration in the present analysis. This assumption leads to constant acceleration rather than constant-thrust maneuvers whose acceleration profiles depend on I . These two are identical in the limit of infinite I , and it is shown in reference 4 that I has little effect on ΔV when maneuvers are compared on the basis of equal burn time (or equivalently, equal average acceleration). Whatever the value of I may be, it is easily shown from equation (2) that the initial and average accelerations are related by

$$A_o = \left[1 - \exp\left(\frac{-\Delta V}{G_\oplus I}\right) \right] \frac{G_\oplus I}{\Delta V} \langle A \rangle \quad (3)$$

This expression may be used to apply the present numerical results to constant-thrust finite I maneuvers by identifying the quoted acceleration levels with $\langle A \rangle$. Moreover, the results apply to both escape and capture maneuvers since A is constant and capture maneuvers, after the convention of reference 4, are integrated backward from the desired orbital power-off point.

Equations of motion. - With the use of the foregoing assumptions, a simple system of differential equations and boundary conditions may be constructed to describe the trajectory. In plane polar coordinates, the trajectory variables (illustrated in fig. 2(b)) are the polar radius R , central angle θ , velocity V , and path angle α relative to the local horizontal. The thrust acceleration is described by its magnitude A (assumed bounded) and angle of attack U_1 (relative to \vec{V}). The force of gravity has a magnitude μ/R^2 and is directed toward the origin. These are transformed to the usual dimensionless variables by dividing radii, velocities, accelerations, and time, respectively, by the radius, local circular velocity, local gravity, and local circular radian period corresponding to the

periapse of the intermediate orbit. Polar angles are measured from the periapse ray of the major axis. The dimensionless variables are denoted by lower case symbols and are related to their physical counterparts by

$$r(\tau) = \frac{R(t)}{R_{pa}} \quad (4a)$$

$$v(\tau) = \frac{V(t)}{V_{c, pa}} \quad (4b)$$

$$a(\tau) = \frac{A(t)}{\left[\frac{\mu}{R_{pa}^2} \right]} \quad (4c)$$

$$\tau = t \frac{V_{c, pa}}{R_{pa}} \quad (4d)$$

$$g = \frac{G}{\left[\frac{\mu}{R_{pa}^2} \right]} = \frac{1}{r^2} \quad (4e)$$

$$v_{\infty} = \frac{V_{\infty}}{V_{c, pa}} \quad (4f)$$

$$\Delta v = \frac{\Delta V}{V_{c, pa}} \quad (4g)$$

These may be used to apply the subsequent results to particular cases. In these units, the first-order vector state equations are

$$\vec{r}' = \vec{v} \quad (5a)$$

$$\vec{v}' = \vec{a} + \vec{g} \quad (5b)$$

or, in component form,

$$r' = v \sin \alpha \quad (6a)$$

$$v' = u_2 a \cos U_1 - \frac{\sin \alpha}{r^2} \quad (6b)$$

$$\alpha' = \frac{u_2 a \sin U_1}{v} + \left(\frac{v^2}{r} - \frac{1}{r^2} \right) \frac{\cos \alpha}{v} \quad (6c)$$

$$\theta' = \frac{v \cos \alpha}{r} \quad (6d)$$

Also, the propulsive effort or Δv is defined by

$$\Delta v = \int_{\tau_0}^{\tau_h} U_2 a \, d\tau \quad (6e)$$

This is the criterion to be minimized. The control variables are the thrust angle of attack U_1 , and the throttle control function U_2 . These are selected (as functions of time) to yield the lowest possible Δv consistent with the boundary conditions to now be derived.

Boundary conditions. - The near-planet end of an escape or capture maneuver terminates in the parking orbit. The boundary conditions appropriate here may be defined in terms of the orbit eccentricity e_{po} and true anomaly ν_{po} of the power-on or power-off point by the well known conic orbit equations (cf. ref. 11):

$$r_0 = \frac{1 + e_{po}}{1 + e_{po} \cos \theta_0} \quad (7a)$$

$$v_0 = \left[\frac{2}{r_0} - (1 - e_{po}) \right]^{1/2} \quad (7b)$$

$$\alpha_0 = \tan^{-1} \left[\frac{e_{po} r_0 \sin \theta_0}{1 + e_{po}} \right] \quad (7c)$$

$$\theta_0 = \nu_{po} \quad (7d)$$

Since the space vehicle would presumably complete several revolutions in the parking orbit, the location ν_{po} of the power-on or power-off point is immaterial from the viewpoint of mission objectives and so can be selected for minimum Δv . Thus, equations (6) define a set of allowable initial conditions with one degree of freedom - namely, ν_{po} .

In addition, the asymptotic boundary conditions must be met at the sphere of influence. That is, for the capture maneuver shown in figure 2(b), the approach hyperbola has a vis-viva energy defined by

$$v_{\infty, h}^2 = v_h^2 - \frac{2}{r_h} = v_{\infty, 2}^2 \quad (8a)$$

where

$$v_{\infty, 2}^2 = \frac{|\vec{V}_{sc, 1} - \vec{V}_{pl, 1}|^2}{V_{c, pa}^2} \quad (8b)$$

and similarly for escape. Further, a geometric constraint of the form

$$\theta_h + \theta_{cst} = \theta_{\infty, 2} \quad (8c)$$

must be satisfied by each maneuver. Again, using the conic relations allows the asymptotic polar angle θ_{cst} for the coasting arc to be written as

$$\theta_{cst} = \varphi_{\infty} - \varphi_h \quad (8d)$$

where

$$\tan \varphi_{\infty} = -hv_{\infty} \quad (8e)$$

$$\tan \varphi_h = \frac{hr_h r'_h}{h^2 - r_h} \quad (8f)$$

and φ_{∞} and φ_h are, respectively, the asymptotic and power-on or power-off true anomalies and h the (constant) angular momentum of the coasting arc. Equations (8) de-

fine a two-degree-of-freedom "target set" of allowable terminal conditions. Its free parameters (v and α) were chosen for convenience in applying the transversality conditions.

Variational Necessary Conditions

The optimal controls $U_1(\tau)$ and $U_2(\tau)$ are defined by Pontryagin's maximum principle, which is developed in reference 10. According to this principle, the controls can be optimal only if the Hamiltonian function

$$\mathcal{H} = \psi_1 r' + \psi_2 v' + \psi_3 \alpha' + \psi_4 \theta' + \psi_5 \Delta v' \quad (9)$$

attains its maximum with respect to $U_1(\tau)$ and $U_2(\tau)$ for $0 \leq \tau \leq \tau_h$. Furthermore, \mathcal{H} is a constant and its value is zero since in the present case the burning time is not constrained. The state variable derivatives are given by equations (6), and the adjoint variables are defined by

$$\psi_1' = - \left[\frac{2 \sin \alpha}{r^3} \psi_2 + \left(\frac{2}{r^3 v} - \frac{v}{r^2} \right) \psi_3 \cos \alpha - \frac{v \cos \alpha}{r^2} \psi_4 \right] \quad (10a)$$

$$\psi_2' = - \left\{ \psi_1 \sin \alpha + \psi_3 \left[\frac{-u_2 a \sin u_1}{v^2} + \left(\frac{1}{r} + \frac{1}{r^2 v^2} \right) \cos \alpha \right] + \psi_4 \frac{\cos \alpha}{r} \right\} \quad (10b)$$

$$\psi_3' = - \left[\psi_1 v \cos \alpha - \psi_2 \frac{\cos \alpha}{r^2} - \psi_3 \left(\frac{v}{r} - \frac{1}{r^2 v} \right) \sin \alpha - \psi_4 \frac{v \sin \alpha}{r} \right] \quad (10c)$$

$$\psi_4' = - \frac{\partial \mathcal{H}}{\partial \theta} = 0, \text{ or } \psi_4 = \text{constant} \quad (10d)$$

$$\psi_5' = - \frac{\partial \mathcal{H}}{\partial \Delta v} = 0, \text{ or } \psi_5 = -1 \quad (10e)$$

(The value of -1 is selected as a scale factor since equations (10) are linear and homogeneous in the ψ_i . The ψ_i may then be interpreted as the partial derivatives of Δv with respect to the terminal values of the corresponding state variables.)

Optimal control laws. - The Hamiltonian may also be written as

$$\mathcal{H} = \left[\psi_1 V \sin \alpha - \psi_2 \frac{\sin \alpha}{r^2} + \psi_3 \left(v^2 - \frac{1}{r} \right) \frac{\cos \alpha}{rv} + \psi_4 \frac{V \cos \alpha}{r} \right] + (U_2 a) \left(\psi_2 \cos U_1 + \psi_3 \frac{\sin U_1}{v} + \psi_5 \right) \equiv F + U_2 a K \quad (11)$$

when equations (6) are substituted into equation (9). Since $U_1(\tau)$ is not constrained, the maximum condition yields

$$\left. \begin{aligned} \frac{\partial \mathcal{H}}{\partial U_1} &= 0 \\ \frac{\partial^2 \mathcal{H}}{\partial U_1^2} &< 0 \end{aligned} \right\} \quad (12)$$

which leads immediately to the optimal steering control law

$$\tan U_1(\tau) = \frac{\psi_3(\tau)}{\psi_2(\tau)v(\tau)} \quad (13)$$

On the other hand, the parameter a is interpreted as the maximum acceleration capability of the vehicle. Thus, $U_2(\tau)$ must be constrained to the range

$$0 \leq U_2 \leq 1 \quad (14)$$

Then since U_2 enters \mathcal{H} linearly, its value must switch discontinuously between zero and wide open according to the sign of the "thrust switching function" K . That is,

$$\left. \begin{aligned} U_2 &= 1 & K > 0 \\ &= 0 & K < 0 \end{aligned} \right\} \quad (15)$$

and is indeterminate in the "singular" case (discussed in appendix A) where $K = 0$ over some finite interval. Thus, aside from the singular case, the optimal trajectories must consist of constant-acceleration and coasting arcs. This conclusion, together with the

previously mentioned fact that capture maneuvers are integrated backward from the desired power-off point, means that escape and capture maneuvers are mathematically identical; the results which will be shown subsequently apply to both cases.

As a point of interest it may be noted that by using equations (13) and (10e), K may be expressed as

$$K = P - 1 \quad (16a)$$

where

$$P = \frac{1}{v} \left(\psi_2^2 v^2 + \psi_3^2 \right)^{1/2} = \left(\psi_2^2 + \frac{\psi_3^2}{v^2} \right)^{1/2} = \frac{\psi_2}{\cos U_1} \quad (16b)$$

Thus, the vector \vec{P} with magnitude P and orientation given by equation (13) is seen to be the "primer vector" of reference 1, expressed in the present coordinate system. Here as in reference 1 the thrust is aligned with the primer and is turned on or off according to whether the magnitude P is greater or less than unity.

Transversality conditions. - Eleven conditions are needed to determine the burning time and to specify the simultaneous solutions of equations (6) and (10). Four of these are given in terms of ν_{po} by equations (7), two are given implicitly in equations (8), one is given by the choice of scale factor in equation (10e), and one more is determinable from the fact that $\mathcal{H} = 0$. The remaining three conditions are obtained by applying the transversality conditions at both the initial and final times. (The partial derivatives needed in applying this condition are presented in appendix B.) At the orbit end this results in

$$\left(\psi_1 \frac{\partial r}{\partial \theta} + \psi_2 \frac{\partial v}{\partial \theta} + \psi_3 \frac{\partial \alpha}{\partial \theta} + \psi_4 \right)_0 = 0 \quad (17)$$

and at the hyperbolic terminal,

$$\left(\psi_1 \frac{\partial r}{\partial v} + \psi_2 + \psi_4 \frac{\partial \theta}{\partial v} \right)_h = 0 \quad (18a)$$

$$\left(\psi_3 + \psi_4 \frac{\partial \theta}{\partial \alpha} \right)_h = 0 \quad (18b)$$

For the case in which θ_∞ is not constrained, these conditions reduce to those presented in reference 4. The adjoint variable ψ_4 (corresponding to the polar angle θ) must then vanish; that is,

$$\psi_4 = \frac{\partial \Delta v}{\partial \theta_h} = 0$$

This further implies that $\psi_{3,h} = 0 = \psi'_{3,h}$ (using eqs. (10c) and (18b) and the relation $(\partial r / \partial v) = -r^2 v$). Thus, in the absence of a geometric constraint, the final thrust direction of an optimal escape or capture maneuver must be tangential to at least second order in $(\tau_h - \tau)$. This explains in part why the tangential steering law ($U_1 \equiv 0$) has been found so close to optimal (in the sense of producing near-minimum values of Δv) for the optimal-angle maneuvers discussed in reference 4.

Optimal Trajectory Solutions

Numerical integration is required to produce solutions in the general finite-thrust case, but analytical solutions may also be derived for the limiting cases of impulsive and ultra-low thrust. These cases are of interest because of the following:

- (1) They furnish upper and lower bounds for finite-thrust performance.
- (2) The impulsive solution in particular provides good physical insight for a surprisingly large range of finite-thrust behavior.
- (3) The impulsive results can further be used to generate a simple but effective feedback solution which may be useful for approximate optimization studies.

These solutions are now presented together with a formal "mean value" result that proves useful in interpreting the numerical finite-thrust data.

Impulsive thrust. - Reference to figure 2(b) shows that for impulsive thrust the powered arc shrinks to a point. In this case, the geometric boundary condition requires that

$$\theta_\infty - \nu_{po} = \theta_{cst} = \varphi_\infty - \varphi_h \quad (19)$$

Thus,

$$\cos(\theta_\infty - \nu_{po}) \equiv D \equiv \cos(\varphi_\infty - \varphi_h) = \cos \varphi_\infty \cos \varphi_h + \sin \varphi_\infty \sin \varphi_h \quad (20)$$

Expanding this expression with the help of the conic relations yields

$$\left. \begin{aligned}
\varphi_h &= \cos^{-1} \left[\frac{\left(\frac{p_h}{r_h} \right) - 1}{e_h} \right] = \sin^{-1} \left\{ 1 - \left[\frac{\left(\frac{p_h}{r_h} \right) - 1}{e_h} \right]^2 \right\}^{1/2} \\
\varphi_\infty &= \cos^{-1} \left(\frac{-1}{e_h} \right) = \sin^{-1} \left(1 - \frac{1}{e_h^2} \right)^{1/2} \\
e_h &= \left(1 + p_h v_\infty^2 \right)^{1/2}
\end{aligned} \right\} \quad (21)$$

squaring, and solving the resulting quadratic for p_h gives the elements of the coasting hyperbola as

$$\left. \begin{aligned}
p_h &= A + \frac{B}{2} \pm \left[B \left(A + \frac{B}{4} \right) \right]^{1/2} \\
e_h &= \left(1 + p_h v_\infty^2 \right)^{1/2}
\end{aligned} \right\} \quad (22)$$

where

$$A = r_h(1 - D)$$

and (23)

$$B = r_h^2 v_\infty^2 (1 - D^2)$$

The velocity and path angle at the impulse point for both the parking orbit and the coasting hyperbola may be computed using equations (7b) and (7c); by the law of cosines the necessary Δv is then

$$\Delta v = \left(v_h^2 + v_o^2 - 2v_h v_o \cos \beta \right)^{1/2} \quad (24)$$

and the law of sines yields

$$\frac{\sin U_{1,o}}{v_h} = \frac{\sin U_{1,h}}{v_o} = \frac{\sin \beta}{\Delta v} \quad (25)$$

where

$$\beta = \alpha_h - \alpha_{po}$$

This is the complete and unique single-impulse solution to the given problem if the initial position ν_{po} is specified in advance. That this solution also satisfies the maximum principle and the terminal transversality condition is now demonstrated. Substituting equations (13) into equation (18b) and the result into equation (18a) yields

$$\psi_{2,h}^* = \frac{-\left(\frac{\partial r}{\partial v}\right)_h}{1 - \frac{v_h \tan U_{1,h}}{\left(\frac{\partial \theta}{\partial \alpha}\right)_h}} \quad (26)$$

$$\psi_3^* = \psi_{2,h}^* v_h \tan U_{1,h} \quad (27)$$

$$\psi_4^* = \frac{-\psi_{2,h}^* v_h \tan U_{1,h}}{\left(\frac{\partial \theta}{\partial \alpha}\right)_h} \quad (28)$$

where the partials are defined in appendix B and the scale factor is temporarily chosen as $\psi_1^* = 1$. Thus, the terminal transversality conditions are satisfied. Next, the previous normalization ($\psi_5 = -1$) may be recovered by computing

$$\psi_5^* = -\left(\psi_{2,h}^{*2} + \frac{\psi_{3,h}^{*2}}{v_h^2}\right)^{1/2} \quad (29)$$

(obtained by setting $K = 0$ in eq. (11) for an optimal impulse) and then dividing $\psi_1^* (=1)$ through ψ_5^* by $-\psi_5^*$.

The adjoint variables ψ_1 , ψ_3 , ψ_4 , and ψ_5 are all constant across an impulse, since their derivatives are bounded (i. e., do not depend on a) and the burning time is infinite.

tesimal. The jump in ψ_2 across an impulse may be obtained by neglecting all terms not dependent on a in equation (10b) and then substituting from equations (6b) and (13):

$$\begin{aligned}\psi_2' &\approx \frac{\psi_3}{v^2} (u_2 a \sin U_1) = \frac{\psi_3}{v^2} v' \tan U_1 \\ &= \frac{\psi_3^2}{\psi_2} \frac{v'}{v^3}\end{aligned}\tag{30}$$

Hence,

$$\psi_2 d\psi_2 = \psi_3^2 \frac{dv}{v^3}$$

The solution of this is

$$\psi_2^2 + \frac{\psi_3^2}{v^2} = \text{constant}\tag{31}$$

It is clear, when recalling equations (16), that the primer P remains constant across an impulse, and if the impulse is optimal with respect to thrust control the constant has unit magnitude. In this case $\psi_2 = \cos U_1$, which in equation (31) implies that $\psi_3 = v \sin U_1$, and this is in turn consistent with equation (13). Thus, it is seen that the closed solution written previously - that is, equations (19) to (24) - satisfies all the necessary conditions of the maximum principle in the case where ν_{po} is fixed.

If ν_{po} is left open, it is necessary in addition to satisfy the initial transversality condition, equation (17). This requires an iterative numerical solution - that is, assuming an initial value of ν_{po} , evaluating equations (19) to (31) and (17), and searching along ν_{po} until equation (17) is satisfied. In the optimal angle case,

$$\psi_4 = \psi_3 = 0$$

Hence,

$$\psi_2 = 1 \quad \text{or} \quad U_1 = 0$$

That is, the impulse is applied tangent to the initial velocity vector. In view of the initial transversality condition (eqs. (17) and (B4)), this impulse is to be applied at the periapse. The corresponding value of Δv is then

$$\Delta v_{\min} = v_h - v_{po} = \left(v_{\infty}^2 + 2 \right)^{1/2} - \left(1 + e_{po} \right)^{1/2} \quad (32)$$

The associated optimal value of θ_{∞} is

$$\theta_{\infty, \text{opt}} = \cos^{-1} \left(-\frac{1}{e_h} \right) \quad (33)$$

where

$$\left. \begin{aligned} e_h &= v_{\infty}^2 + 1 \\ p_h &= 1 + e_h \end{aligned} \right\} \quad (34)$$

Mean value solution. - Although numerical methods must be used to obtain the general, finite-thrust trajectories, a formal solution for Δv can be obtained by converting the velocity equation (eq. (6b)) into an energy equation. Multiplying by v and using equation (6a) yield

$$vv' + \frac{r'}{r^2} = u_2 a v \cos U_1 \quad (35)$$

or, recalling equation (8a),

$$\left(\frac{v^2}{2} \right)' = u_2 a v \cos U_1 \quad (36)$$

Applying the law of the mean to the right side of equation (36) gives

$$\Delta v = \frac{v_{\infty, h}^2 - v_{\infty, po}^2}{2 \langle v \cos U_1 \rangle} \quad (37)$$

where

$$\langle v \cos U_1 \rangle = \frac{1}{\tau_h} \int_{\tau_0}^{\tau_h} v \cos U_1 \, d\tau \quad (38)$$

and the initial vis-viva energy $v_{\infty, po}^2$ is given by

$$v_{\infty, po}^2 = e_{po} - 1 \quad (39)$$

Thus, Δv may be expressed as the ratio of the energy increment between the initial orbit and the asymptotic boundary conditions to the mean path velocity component in the direction of thrust. As the energy increment is fixed, it is clear that the control action seeks to maximize $\langle v \cos U_1 \rangle$, which is the mean rate of energy addition to the space vehicle. The ratio of Δv 's for finite and impulse thrust, which is termed a "velocity correction factor", is thus given by

$$f_v = \frac{\Delta v_{act}}{\Delta v_{imp}} = \frac{\langle v \cos U_1 \rangle_{imp}}{\langle v \cos U_1 \rangle_{act}} \quad (40)$$

This factor is often used to account for gravity losses (e.g., a wide range of data of this kind is presented in ref. 4). Nevertheless, it is evident that control actions and the choice of initial conditions will have an explicit effect on f_v whether a gravitational field is present or not. Thus, f_v in general represents steering losses as much as gravity losses.

Microthrust. - An approximate but useful solution for the low-thrust case is suggested by the previous result. It is noted, first, that the energy increment in equation (37) does not depend essentially on the shape of the initial orbit. For any elliptic orbit (whose periape radius $r_{pa} = 1$), a circular orbit having the same energy (and period) in absolute units has the radius

$$r_{c, equivalent} = \frac{1}{1 - e_{po}} \quad (41)$$

The results of reference 4 indicate that the value of $\langle v \cos U_1 \rangle$ does not depend strongly on e_{po} for the low-thrust spirals. Thus, the familiar "expanding circle" approximation now takes the form

$$\Delta v_{microthrust} = v_{\infty, h} + (1 - e_{po})^{1/2} \quad (42)$$

(The quantity $(1 - e_{po})^{1/2}$ may be recognized as the circular velocity of the equal-energy circular orbit.) This in combination with equation (32) yields

$$f_{v, \text{microthrust}} \approx \frac{v_{\infty, h} + (1 - e_{po})^{1/2}}{(v_{\infty, h}^2 + 2)^{1/2} - (1 + e_{po})^{1/2}} \quad (43)$$

Note that the result expressed in equation (43) does not depend on the asymptotic direction θ_{∞} . By contrast, θ_{∞} enters explicitly in the impulsive solution (eqs. (19) to (25)). Hence, it may be anticipated that the effect of asymptotic direction constraints will be progressively less important as the vehicle acceleration level decreases.

Variational solutions for finite thrust. - The trajectory and adjoint equations (eqs. (6) and (10)), the optimal control laws (eqs. (13) and (15)), and the transversality conditions (eqs. (17) and (18)), together with the necessary auxiliary relations, were programmed for numerical solution on a digital computer. As previously mentioned, each particular case is solved iteratively as a two-point boundary value problem. Each trial integration involves 11 subsidiary conditions, of which 6 are stated as physical boundary conditions, 3 are given in terms of the transversality conditions, 1 is incorporated in the choice of scale factor, and the last is determined by the fact that $\mathcal{H} = 0$. Note that some of these conditions apply at the initial time and some at the final time. A solution to this problem is defined by a complete set of initial conditions which lead, by means of equations (6), (10), (13), and (15), to the desired terminal conditions.

The following procedure is used to accomplish the necessary three-dimensional search (using ν_{po} , $U_{1,0}$, and ψ_4^* as search variables). Equations (17) and (13) are inverted to yield

$$\psi_{2,0}^* = \frac{-\left(\frac{\partial r}{\partial \theta} + \psi_4^*\right)}{\frac{\partial v}{\partial \theta} + \frac{\partial \alpha}{\partial \theta} v_0 \tan U_{1,0}} \quad (44)$$

when resorting to the normalization $\psi_{1,0}^* = 1$. The partials (see appendix B) may be computed since ν_{po} is known. Then

$$\psi_{3,0}^* = \psi_{2,0}^* v_0 \tan U_{1,0} \quad (45)$$

Finally, ψ_5^* is computed to make $\mathcal{H} = 0$ (see eq. (11)) and is used to renormalize so that $\psi_5 = -1$. With this, all initial values are defined. Integration is stopped when the desired value of v_{∞}^2 is attained (see eq. (8a)); this defines the final time τ_h . A terminal error function is constructed to give a measure of error in the remaining conditions; that is,

$$E = \mathcal{E}_1^2 + \mathcal{E}_2^2 + \mathcal{E}_3^2 \quad (46)$$

where \mathcal{E}_1 and \mathcal{E}_2 are, respectively, the left sides of equations (18a) and (18b) and (from eqs. (8c) and (8d))

$$\mathcal{E}_3 = \theta_\infty - \left[\theta_h + (\varphi_h - \varphi_\infty) \right]$$

is the error in asymptotic direction. A multivariable search routine similar to that described in reference 12 is used to drive E to zero. Rapid convergence depends on making reasonably good initial guesses for ν_{po} , $U_{1,0}$, and ψ_4 . The choice of ν_{po} , $U_{1,0}$, and ψ_4 as search variables results in several advantages. First, they are bounded, which means that an exhaustive search could be made. This is important from the convergence viewpoint and also because no uniqueness theorem is available for the present nonlinear type of problem. Secondly, these variables have definite physical meanings, which are the same whether finite or impulsive thrust is used. Thus, it is often possible to obtain adequate initial guesses by inspecting the easily obtained impulsive results.

Near-optimal feedback solutions. - Even when the previous techniques are used, the "exact" variational solution technique requires a sophisticated computing facility and significant amounts of machine time. A less exact but faster and more flexible technique is developed in appendix C. It relies on a nonoptimal but stable and strongly convergent feedback algorithm to satisfy the problem's boundary conditions. Near-minimum Δv 's are then obtained by direct numerical optimization of adjustable parameters in the feedback loop. Comparisons with the variational results indicate that the true minimum propulsive velocity increment can be approached within small fractions of 1 percent with relative ease. Hence, the feedback technique of appendix C could be used effectively in those cases where minor deviations from the true minimum Δv can be accepted.

Matching Conditions for Combined Maneuvers

The considerations presented above lead to escape or capture maneuvers which yield minimum Δv for prescribed values of v_∞ and θ_∞ . But to solve the originally stated problem, it is also necessary to join pairs of escape and capture maneuvers in such a way that (1) the geometric constraint illustrated in figure 2(b) is satisfied, that is,

$$\theta_{\infty,1} + \theta_{\infty,2} = \Theta = \cos^{-1} \left(\frac{\vec{v}_{\infty,1} \cdot \vec{v}_{\infty,2}}{v_{\infty,1} v_{\infty,2}} \right) \quad (47)$$

and (2) the sum

$$\sum_1^2 \Delta v_i = \Delta v_1 + \Delta v_2 = \text{minimum} \quad (48)$$

When it is assumed that $v_{\infty, 1}$ and $v_{\infty, 2}$ have been determined by prior interplanetary trajectory calculations, the values of Δv depend only on θ_{∞} ; that is,

$$\sum_1^2 \Delta v_i = \Delta v_1(\theta_{\infty, 1}) + \Delta v_2(\theta_{\infty, 2}) \quad (49)$$

Thus, it is necessary only that

$$d\left(\sum_1^2 \Delta v_i\right) = \frac{\partial \Sigma \Delta v}{\partial \theta_{\infty, 1}} d\theta_{\infty, 1} + \frac{\partial \Sigma \Delta v}{\partial \theta_{\infty, 2}} d\theta_{\infty, 2} = 0$$

or, using equation (49),

$$\frac{\partial \Delta v_1}{\partial \theta_{\infty, 1}} d\theta_{\infty, 1} + \frac{\partial \Delta v_2}{\partial \theta_{\infty, 2}} d\theta_{\infty, 2} = 0 \quad (50)$$

To satisfy the boundary condition it is necessary that

$$d\Theta = d\theta_{\infty, 1} + d\theta_{\infty, 2} = 0 \quad (51)$$

Hence, equation (50) becomes

$$\frac{\partial \Delta v_1}{\partial \theta_{\infty, 1}} = -\frac{\partial \Delta v_2}{\partial \theta_{\infty, 2}} \quad (52)$$

Now since θ_{∞} is a function of θ_h , φ_h , and φ_{∞} (see eqs. (8d) to (8f)), Δv may be written as composite function of those variables; that is,

$$\Delta v = \Delta v(\theta_h, \varphi_h, \varphi_{\infty})$$

and thus

$$\frac{\partial \Delta v}{\partial \theta_{\infty}} = \frac{\partial \Delta v}{\partial \theta_h} \frac{\partial \theta_h}{\partial \theta_{\infty}} + \frac{\partial \Delta v}{\partial \varphi_h} \frac{\partial \varphi_h}{\partial \theta_{\infty}} + \frac{\partial \Delta v}{\partial \varphi_{\infty}} \frac{\partial \varphi_{\infty}}{\partial \theta_{\infty}}$$

As is seen from equation (8c),

$$\frac{\partial \theta_h}{\partial \theta_{\infty}} = 1$$

while from equations (8e) and (8f)

$$\frac{\partial \varphi_h}{\partial \theta_{\infty}} = \frac{\partial \varphi_{\infty}}{\partial \theta_{\infty}} = 0$$

Hence,

$$\frac{\partial \Delta v}{\partial \theta_{\infty}} = \frac{\partial \Delta v}{\partial \theta_h} = \psi_4$$

and equation (52) reduces to the simple requirement that

$$\psi_{4,1} = \psi_{4,2} \quad (53)$$

This condition could also have been obtained by considering the problem as a whole. But then it would have been necessary to derive "jump conditions" for the ψ_i (similar to those required for state variable inequality constraints, see ref. 10) to ensure that the desired orbit was actually attained. The present approach of matching individually optimal sub-trajectories by means of equation (53) not only represents a considerable practical simplification from the computational viewpoint, but it also produces a range of optimal single trajectories that may be of interest in themselves (e. g. , for a one-way orbiting probe mission in which the location of the parking orbit periapse has been prescribed on the basis of mission observational requirements).

RESULTS AND DISCUSSION

As previously stated, elliptic parking orbits are currently of interest because they offer a large reduction of the propulsive effort or Δv when used in place of the more

familiar circular orbit. Comparing the values of equation (32) with $e_{po} = 0$ (circular orbit) and $e_{po} \rightarrow 1.0$ (a highly eccentric ellipse) shows that the saving may approach 41.4 percent of the reference circular velocity for unconstrained geometry (θ_∞ open). This saving is especially important for trips to the major planets, which have strong gravitational fields and hence high circular velocities. At Jupiter, for instance, where $V_c \approx 40$ kilometers per second, the ΔV for a typical capture maneuver (per ref. 7) may be reduced from 18 or 19 to 2 or 3 kilometers per second. This will clearly have an enormously beneficial effect on vehicle weight.

On the other hand, the long periods and limited times at low altitude associated with highly eccentric orbits may create difficulties in carrying out scientific observations of the destination planet. Yet these represent the very purpose and justification for the mission. Thus it may be expected that the value of e_{po} finally chosen will reflect a compromise between propulsive effort and observational requirements. In figure 3, the Δv

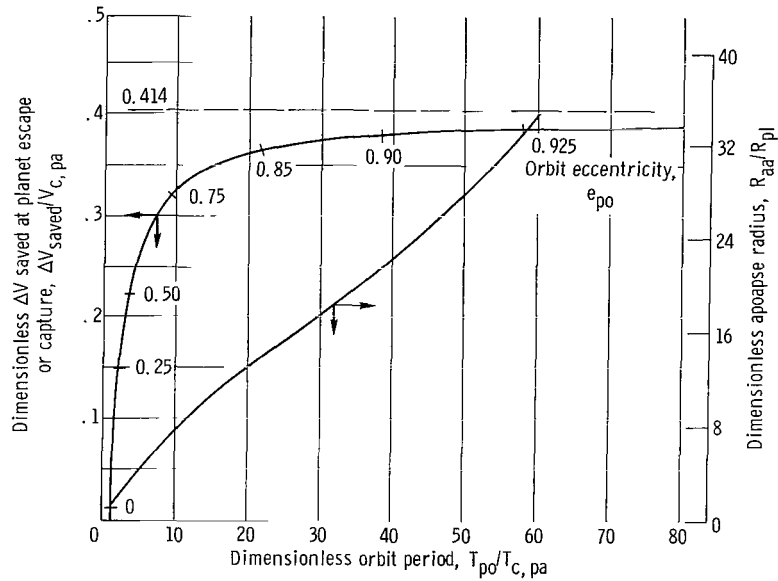


Figure 3. - Relation of parking orbit parameters to mission velocity increments. Unconstrained maneuvers; impulsive thrust, $R_{pa}/R_{pl} = 1.10$.

saving and the orbit apoapse radius are plotted as functions of the orbit period. The eccentricity e_{po} is indicated by markers along the two curves. There is evidently little further Δv reduction for $e_{po} > 0.9$, yet both the period and apoapse radius increase very rapidly beyond this point. The value of $e_{po} = 0.9$ therefore appears to be a reasonable choice and is used for illustrative purposes in the remainder of this discussion.

Individual Escape or Capture Maneuvers

The individual maneuvers are of interest in themselves (i.e., for an orbiting probe mission) in addition to being part of the "destination planet problem" for a round trip. Unfortunately, Δv 's as low as those predicted by equation (32) are not always available because of (1) the effect of a constraint on θ_∞ (the optimal value per eq. (33) does not in general match the problem geometry) and (2) the ΔV penalty due to finite thrust (generally the propulsive efficiency is reduced when an impulse is replaced by finite thrust). These effects are now considered.

Effect of asymptotic direction. - Constraints on θ_∞ arise regularly as part of the round-trip problem and may also occur in probe missions if observational requirements dictate a particular orbit shape and orientation. The effects of constraining θ_∞ are illustrated in figure 4 for a relatively low-energy maneuver in which $v_\infty = 0.25$. In figure 4(a), the characteristic velocity ratio f_v (propulsive ΔV divided by ΔV_{\min}) is plotted against θ_∞ for acceleration levels ranging from impulsive (the lower curve) to 0.01 local gravity. Clearly, the impulsive limiting solution does represent a lower bound of performance for all finite-thrust cases. For impulsive thrust, the minimum value of 1 for f_v occurs at $\theta_\infty = 2.8$ radians as predicted by equation (33). This case represents tangential firing at periapse. A maximum value of $f_v = 5.8$ occurs at $\theta_\infty = 5.2$ radians; this maneuver consists of firing tangentially at the apoapse. For intermediate cases, the impulse does not occur at an apse and is not tangential. Ratioing the values of equation (32) for $e_{po} = 0$ and 0.9 shows that an equivalent value of f_v for a circular orbit is about 7.3. Thus, there is always some saving for the elliptic orbit even when the worst possible value of θ_∞ is required.

A comparison of this impulsive solution (in which f_v represents steering losses only) with the optimal-angle results of reference 4 (where f_v only includes gravity losses) indicates that these two effects can lead to similar performance penalties. In general, however, f_v includes both effects simultaneously, and the particular manner in which they combine is a major concern of this report.

Passing to the finite-thrust cases in figure 4(a), it is seen that dimensionless acceleration as low as $a = 0.01$ yield a performance that does not differ markedly from impulsive except in the immediate vicinity of the optimal-angle condition ($\theta_\infty \approx 2.8$ rad). For $a = 0.01$, the minimum of 1.38 for f_v occurs at the same value of θ_∞ . Except within ± 0.5 radian of this value, the results for $a = 0.01$ cannot be distinguished from these for impulsive thrust. But when $a \lesssim 0.001$, the results (not illustrated here) begin to resemble the "microthrust" solution (eqs. (42) and (43)). Thus, for low-thrust systems, the results do not so depend strongly on θ_∞ . But for medium- or high-thrust systems ($a = 0.01$), the ΔV requirement is dominated by θ_∞ and is relatively insensitive to thrust level; that is, gravity losses and steering losses are not directly additive. Hence,

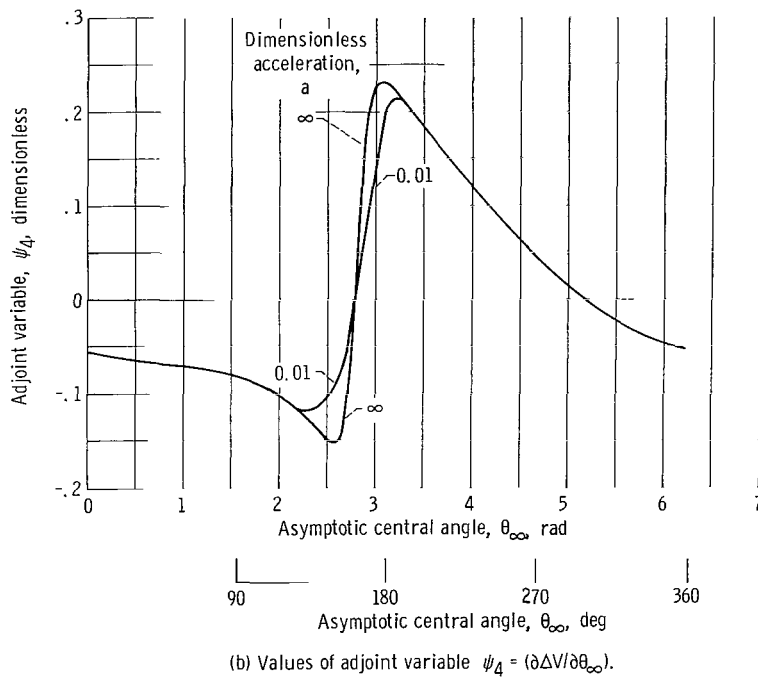
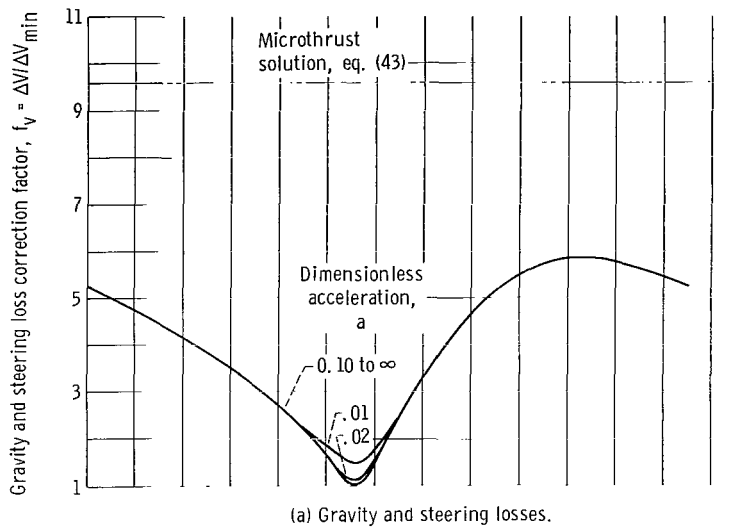
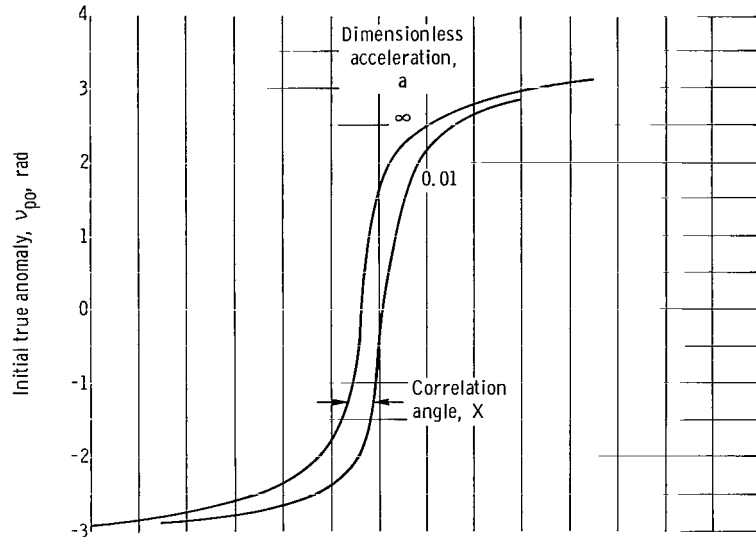
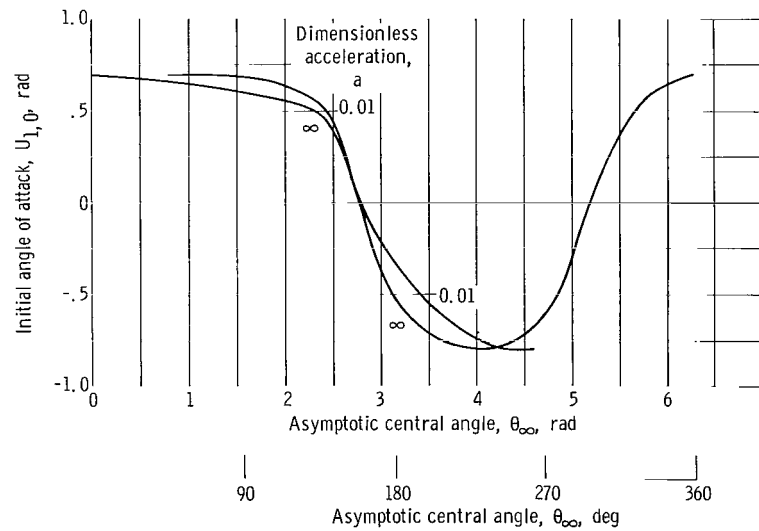


Figure 4. - Effects of asymptotic direction constraints on orbit-escape maneuvers. Parking orbit eccentricity, $e_{p0} = 0.9$; asymptotic velocity, $V_\infty = 0.25 V_C$, pa; constant acceleration.



(c) True anomaly at power-on point.



(d) Initial angle of attack.

Figure 4. - Concluded.

it appears likely that the effects of constrained θ_∞ could be offset at least partially by using a much smaller engine system than would normally be expected. This possibility is illustrated later.

Parts (b), (c), and (d) of figure 4 illustrate the optimal values of the search variables discussed previously. In figure 4(b) the adjoint variable ψ_4 is plotted against θ_∞ ; it simply reflects the slope of the curves shown in figure 4(a). The initial true anomaly ν_{po} and initial angle of attack $U_{1,0}$ are then shown in figures 4(c) and (d). Because of the similarity in shape of these curves, good initial guesses for finite thrust ψ_4 , $U_{1,0}$, and

v_{po} can be obtained from impulsive data, that is,

$$v_{po}(\theta_\infty)_{\text{finite thrust}} \approx v_{po}(\theta_\infty - X)_{\text{impulsive thrust}} \quad (54)$$

where the correlation angle X is about 0.25 radian for the case illustrated in figure 4(c). Values of X appropriate for other values of a and v_∞ can be obtained by comparing any one converged finite-thrust case to the impulsive data. In this fashion a finite-thrust "performance map", such as figure 4, can be generated without major computational difficulties.

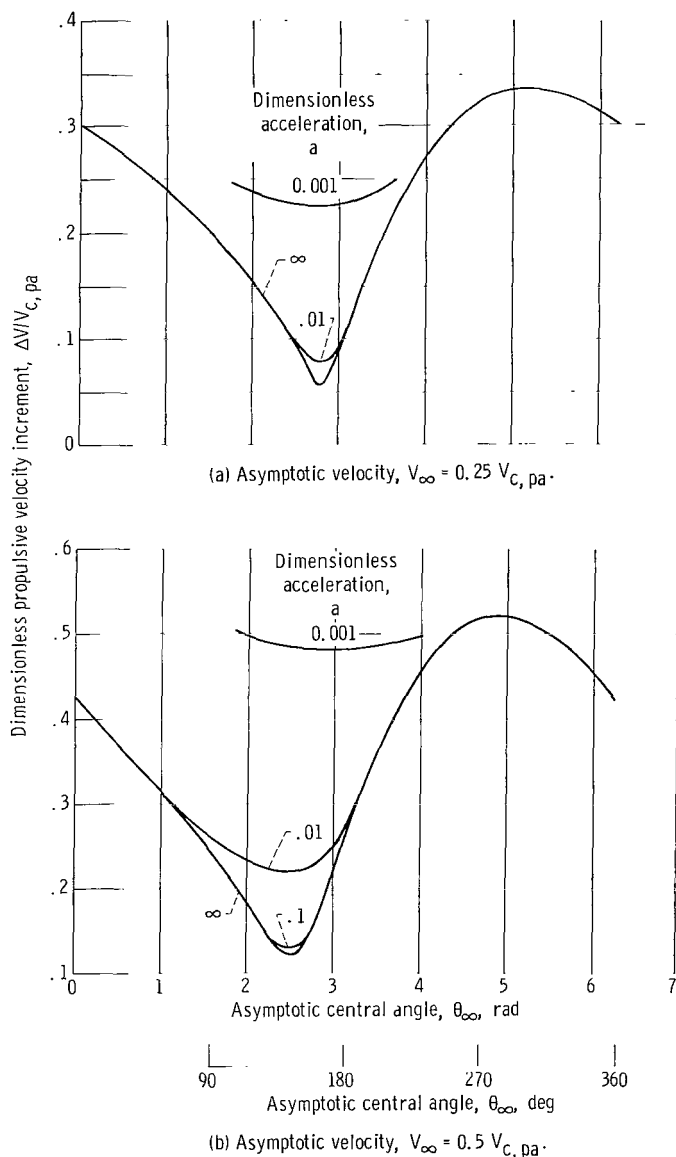
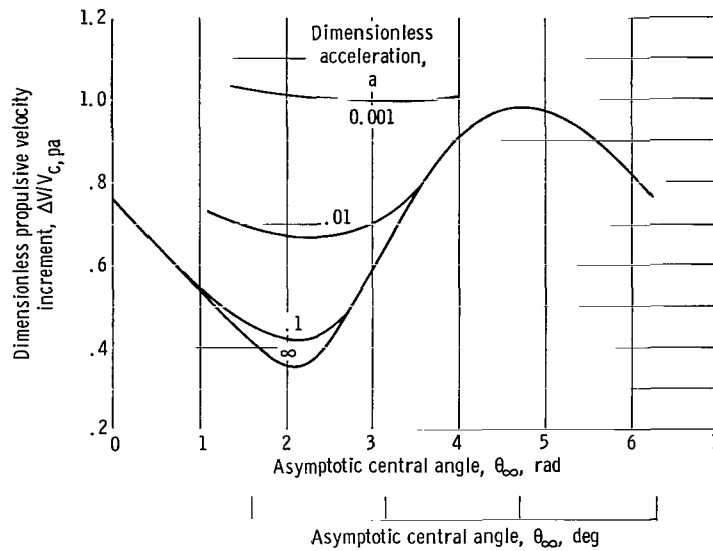


Figure 5. - Comparison of impulsive and finite-thrust maneuvers.



(c) Asymptotic velocity, $V_\infty = 1.0 V_{c, pa}$

Figure 5. - Concluded.

Effect of asymptotic velocity. - Figure 5 illustrates the $\Delta V/\theta_\infty$ characteristic for values of v_∞ of 0.25, 0.50, and 1.0, and for accelerations of 0.001, 0.01, 0.1, and impulsive. The results are now presented in terms of $\Delta v \equiv \Delta V/V_{c, pa}$ (rather than in terms of $f_v \equiv (\Delta V/\Delta V_{min})$) so that the Δv 's for different values of v_∞ are made dimensionless by the same base number. Aside from this change of base, figure 5(a) represents the same low-energy maneuvers ($v_a = 0.25$) that were just described. In comparison with this, the higher energy trajectories portrayed in figures 5(b) and (c) display (1) generally higher Δv levels, (2) less relative variation between the impulsive maxima and minima, and (3) a greater separation between the impulsive and low-thrust curves. From this, it is concluded that the effects of finite thrust are increasingly more important for high-energy maneuvers; that is, the gravity losses are proportionately larger and extend over a wider range of θ_∞ . Nevertheless, it is still true that gravity losses and steering losses do not add directly together. As previously mentioned, the effects of constraints on θ_∞ can be offset to some degree by using a relatively low acceleration and hence a small and presumably light engine.

Characteristics of finite-thrust trajectories. - In figure 6 are presented some typical state and control variable histories for maneuvers where $a = 0.01$ and $v_\infty = 0.25$. Figure 6(a) represents the optimal angle case where θ_∞ is allowed to take on its most advantageous value of about 2.8 radians. The state variables r , v , and α , the angle of attack control variable U_1 , and the thrust switching function K are plotted against the polar angle θ from ν_{po} to θ_∞ . The powered arc is indicated by the solid portion of the

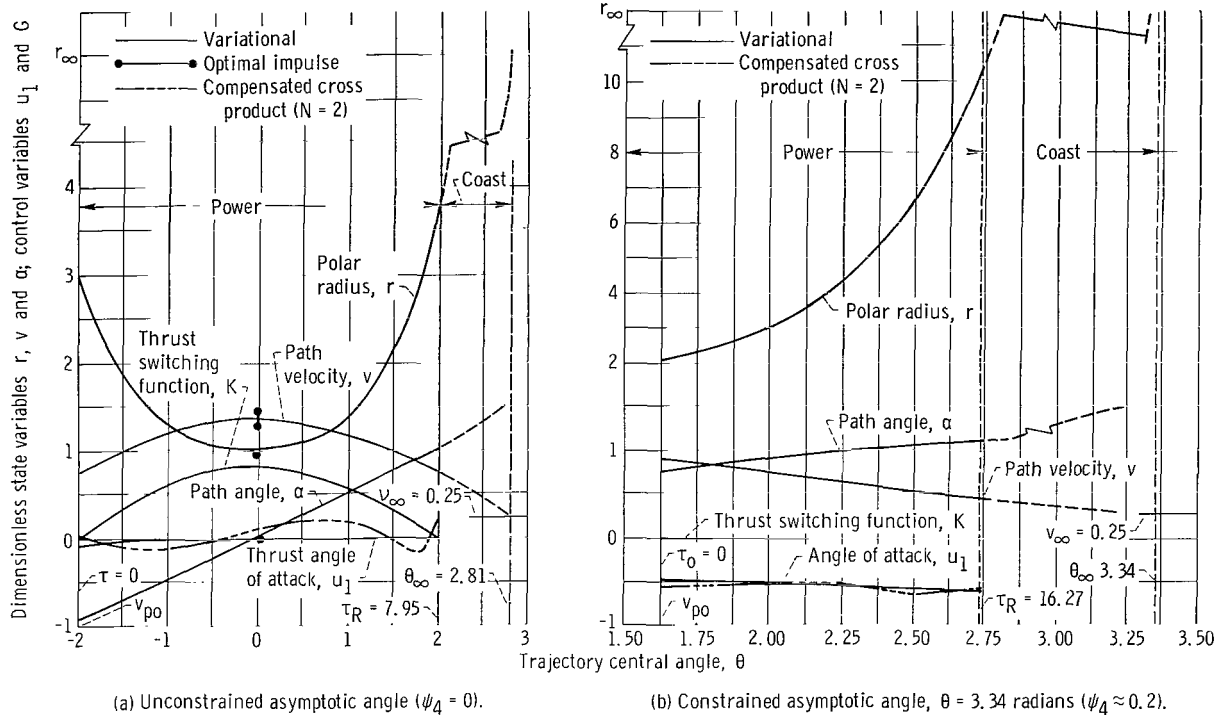


Figure 6. - Characteristics of finite-thrust trajectories. Parking orbit eccentricity, $e_{po} = 0.9$; dimensionless acceleration, $a = 0.01$; dimensionless hyperbolic velocity, $v_\infty = 0.25$.

curves while the subsequent coasting arc is dashed. (The dash-dotted curves are discussed in appendix C.)

It is clear that in this case there is very little steering action. That is, U_1 is only slightly different from zero (tangential thrust) at the beginning and approaches this condition ever more closely as the maneuver proceeds. (It was shown in ref. 4 that tangential steering is always a close approximation to the optimal when θ_∞ is not constrained.) Here $\cos U_1 = 1$ throughout the maneuver, but $\langle v \rangle$ is seen to be appreciably lower than for the impulsive case denoted by heavy dots. Hence (recalling eq. (40)), the Δv is increased by some 38 percent. The thrust switching function begins at zero, increases to a sizable positive value during the midportion of the trajectory, and then decreases to zero again at τ_h - that is, just as the prescribed asymptote is attained. The thrust control U_2 , which had unit magnitude from $\tau = 0$ to τ_h , is then zero during the final part of the trajectory in which the vehicle coasts to the sphere of influence.

Figure 6(b) presents the same data for a constrained trajectory, that is, $\theta_\infty = 3.334$ radians ($\psi_4 = 0.2$). Although this is only about 30° beyond the optimal angle, the trajectory is evidently quite different in all respects. There is a pronounced steering action in this case ($U_1 \approx -0.55$ rad), which in addition to the late power-on point (about 1.6 rad after periapse) provides the extra 30° of turning. This is obtained, however, at the expense of doubling the Δv as compared to the previous case. That is, with both v and

$\cos U_1$ low throughout the maneuver, the mean value $\langle v \cos U_1 \rangle$ is also low and (recalling eq. (40)) Δv is therefore large. In this case, however, there is little difference in Δv for the impulsive and finite-thrust cases.

It is of interest to note the behavior of the thrust switching function K in this case. As figure 6(b) shows, its magnitude is very small throughout the entire trajectory. It is believed, however, that this is not a singular arc in the mathematical sense discussed in appendix A because of the following two reasons:

(1) Although it cannot be illustrated to the scale of figure 6(b), K in this case has the same characteristic arched shape as in figure 6(a) - except scaled down by about three orders of magnitude. The peak value of around 10^{-3} is considered significant in comparison to the roundoff errors of numerical integration. The effects of the latter may be judged by the fact that \mathcal{H} , which is supposed to be constant and was initially set to zero, was observed to fluctuate randomly between $\pm 10^{-7}$. In this case, K contributed about 10^{-5} to \mathcal{H} ($=F + U_2 aK$) and is thus significant by two orders of magnitude.

(2) In addition to the fact that K behaves qualitatively as it should, there is a ready physical explanation for its observed low quantitative magnitude: As may be recalled from figure 4(a) or 5(a), the Δv is quite insensitive to acceleration outside a $\pm 30^\circ$ band centered on $\theta_{\infty, \text{opt}}$. That is, for trajectories with strong geometric constraints it simply does not matter what thrust is used in the range $0.01 \leq a < \infty$. As may be seen in the figure, the powered trajectory takes place at rather high radii ($2 \leq r \leq 10.3$) where the gravitational attraction ($1/r^2$) is weak. At a high enough radius, even 0.01 g behaves as an impulse, and for an impulse $K = 0$. (Note that the acceleration ratio in the present example would vary from 0.04 to about 1.1 if referenced to the local rather than the periapse gravity field.)

Thus, it is concluded that this trajectory also is locally optimal with respect to thrust control. A study of other cases (not illustrated) suggests that this behavior is quite typical of heavily constrained trajectories in general.

Combined Trajectories

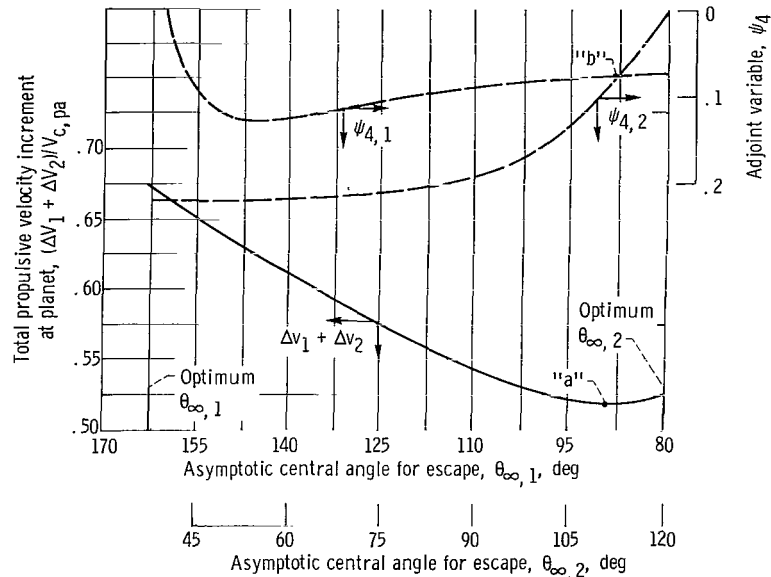
The main features of individual maneuvers have been indicated, but it remains to combine them so as to form an optimal overall trajectory described by the parameters $V_{\infty, 1}$, Θ , and $V_{\infty, 2}$ (recall fig. 2(a)).

Matching procedure. - As shown in the analysis, optimal matching is attained when the following two conditions are satisfied:

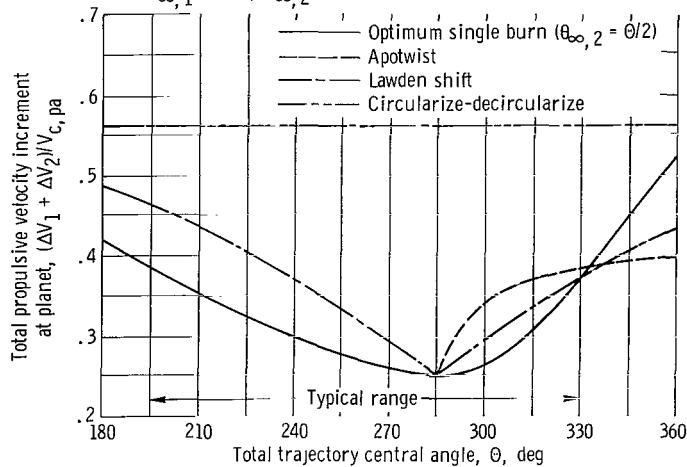
$$\theta_{\infty, 1} = \Theta - \theta_{\infty, 2} \quad (55a)$$

$$\psi_{4,1} = \psi_{4,2} \quad (55b)$$

Equations (55) can be satisfied without an iterative search by aligning the escape and capture ψ_4 against θ_∞ curves (see fig. 4(b)) in a "back-to-back" fashion, so that the sum of ordinates is constant and equal to Θ . The necessary value of $\psi_{4,1} = \psi_{4,2}$ is then read directly from the intersection. This is illustrated in figure 7(a) for an impulsive thrust case in which $v_{\infty,1} = 0.25$, $v_{\infty,2} = 1.00$, and $\Theta = 200^\circ$ or 3.5 radians (about 80°



(a) Effect of parking orbit orientation. Hyperbolic velocities, $v_{\infty,1} = 0.25$, $v_{\infty,2} = 1.00$.



(b) Comparison of several types of approach and departure maneuvers. Parking orbit eccentricity, 0.9; hyperbolic velocities, $v_{\infty,1} = v_{\infty,2} = 0.5 V_C$, pa.

Figure 7. - Combined maneuvers at destination (impulsive ΔV 's). Angle between hyperbolic asymptotes, $\Theta = 3.5$ radians (200°).

less than the optimal value defined by eq. (33)). The total propulsive $\Delta v_1 + \Delta v_2$ and the adjoint variables $\psi_{4,1}$ and $\psi_{4,2}$ are plotted against $\theta_{\infty,1}$ and $\theta_{\infty,2}$ (note that $\theta_{\infty,1}$ and $\theta_{\infty,2}$ sum to 200° everywhere) over the range from optimal-angle capture to optimal-angle escape. The minimum value of $\Delta v_1 + \Delta v_2$ (point a) and equality of $\psi_{4,1}$ and $\psi_{4,2}$ clearly occur at the same values of $\theta_{\infty,1}$, namely 112° . The corresponding $\theta_{\infty,2}$ is then 88° . In general, the optimal distribution of Θ between $\theta_{\infty,1}$ and $\theta_{\infty,2}$ tends to favor the high-energy maneuver; it becomes more nearly even (i. e., $\theta_{\infty,1} \rightarrow \theta_{\infty,2}$) as $v_{\infty,1} \rightarrow v_{\infty,2}$. In figure 7(b), the effect of Θ itself is illustrated for pairs of impulsive maneuvers where $v_{\infty,1} = v_{\infty,2} = 0.5$. The lower solid curve represents trajectories using single-burn maneuvers; every point on this curve was obtained by the previous method. The minimum occurs at $\theta = 286^\circ$, which is compatible with the values of $\theta_{\infty,1}$ and $\theta_{\infty,2}$ ($\approx 143^\circ$) called for by equation (33) in the optimal-angle case.

Comparison of single- and multiple-burn maneuvers. - So far, only single-burn maneuvers have been considered. But from references 5 to 7 it is known that alternative multiburn maneuvers exist which may also give low Δv . Figure 7(b) also presents an impulsive Δv comparison between optimal single-burn and typical multiburn trajectories. In general, the multiburn trajectories consist of optimal-angle escape and capture together with one or more auxiliary maneuvers to reorient the ellipse. That is, the mismatch angle $\sigma = \Theta - \Theta_{\text{opt}}$ is accommodated by rotating the ellipse major axis in the orbit plane or by twisting the orbit plane about the major axis.

For instance, the "circularize-decircularize" maneuver (ref. 5) whose performance is indicated by the upper curve, involves two extra maneuvers: (1) an impulse at apoapse to attain a circular orbit with coasting to make up the angle σ ; and (2) a retro-impulse to regain the original eccentricity but with the line of apsides now rotated through the angle σ . For this sequence of maneuvers the required auxiliary Δv (in addition to the optimal-angle escape and capture Δv 's) is

$$\Delta v_{\text{aux}} = 2(v_{c,aa} - v_{aa}) \quad (56)$$

Lawden's shift maneuver (ref. 1) may be regarded as an optimized version of the above, utilizing transfer by an intermediate ellipse rather than a circle. Its performance is illustrated by the symmetric broken curve in figure 7(b), the Δv shift penalty is given approximately by

$$\Delta v_{\text{aux}} \approx 2(v_{c,aa} - v_{aa}) \sin \left| \frac{\sigma}{2} \right| \quad (57)$$

The "apotwist" maneuver (ref. 5) shown by the dotted curve is essentially different in that the orbit is not in the plane of the \vec{v}_∞ 's. It involves only one extra maneuver which occurs

at apoapse and serves to rotate the orbit plane about the major axis. In this case, the Δv penalty is

$$\Delta v_{\text{aux}} = 2v_{\text{aa}} \sin \frac{\omega}{2} \quad (58)$$

where

$$\cos \omega = \frac{\cos(\Theta - \pi) + \sin\left(\theta_{\infty, 1, \text{opt}} - \frac{\pi}{2}\right) \sin\left(\theta_{\infty, 2, \text{opt}} - \frac{\pi}{2}\right)}{\cos\left(\theta_{\infty, 1, \text{opt}} - \frac{\pi}{2}\right) \cos\left(\theta_{\infty, 2, \text{opt}} - \frac{\pi}{2}\right)}$$

This maneuver is applicable only when $\sigma > 0$. All of these multiburn maneuvers share the feature that $\Delta v_{\text{shift}} \rightarrow 0$ as $e_{\text{po}} \rightarrow 1$, for then $V_{c, \text{aa}}$ and V_{aa} both $\rightarrow 0$. Thus, the Δv penalty for nonoptimal Θ can be made arbitrarily small by first using one further impulse as periapse to attain $e_{\text{po}} \approx 1$. There is then no Θ penalty, and the Δv for raising e_{po} is recovered in the final escape maneuver. Unfortunately, all this requires a great deal of time; the global optimum (zero penalty for constrained Θ) is attainable only in the limit of infinite maneuver time. The data shown in figure 7(b) are for the case where e_{po} is not changed. Even so, the apse shift maneuvers still involve some time increment beyond that required for single-burn maneuvers. This increment, roughly proportional to σ , should be counted as a mission penalty unless useful observations can be made during the long, high radius coasts. (The apotwist maneuver has no time penalty if e_{po} is not changed but can only be used if $\sigma > 0$.)

It is noted that in all the preceding cases the Δv shift penalty does not depend on v_{∞} and thus will be comparatively small for very energetic trajectories. Also, for any energy level the multiburn maneuvers do seem to offer advantages when Θ is severely constrained. They should be seriously considered whenever a "difficult" value of Θ (e.g., 360°) cannot be avoided, especially with high-energy maneuvers.

On the other hand, the single-burn scheme is always superior in the immediate vicinity of $\Theta = \Theta_{\text{opt}}$. This is because equation (53) implies

$$\left. \frac{d(\Delta v_1 + \Delta v_2)}{d\Theta} \right|_{\Theta_{\text{opt}}} = \psi_{4, 1, \text{opt}} + \psi_{4, 2, \text{opt}} = 0 \quad (59)$$

which is clearly not the case for the multiburn maneuvers as they are presently conceived.

Sample Application

The foregoing results can be most readily appreciated by considering a specific mission. A good example for this purpose is the 1400-day Jupiter round trip with 200 days of stay time illustrated in figure 1 and discussed in reference 7. This mission is of interest because it evidently presents the lowest velocity increment sum ($\Sigma\Delta v$) of any Jupiter round trip in which a low periapse elliptic parking orbit is used. Although the trip time may seem uncomfortably long (a representative Mars or Venus trip takes about 500 days), there is a substantial increase in $\Sigma\Delta v$ for going to the next lower feasible trip time of 1000 days. The 200-day stay at Jupiter would at least provide ample time to carry out a significant amount of scientific investigation.

The planetocentric maneuver data pertaining to this mission were obtained from reference 7:

$$V_{\infty,1} = V_{\infty,2} \approx 10.00 \text{ km/sec}$$

$$\Theta = 4.94 \text{ rad}$$

Since $V_{c,2} \approx 40$ kilometers per second (the reference periapse radius is taken to be $1.125 R_1$), the dimensionless hyperbolic velocities are

$$v_{\infty,1} = v_{\infty,2} = 0.25$$

Since the asymptotic speeds are equal and it is assumed that $a_{\text{cap}} = a_{\text{esc}}$, the matching condition (eq. (55)) shows immediately that Θ should be divided equally between the capture and escape maneuvers. Then

$$\theta_{\infty,1} = \theta_{\infty,2} = 2.47 \text{ rad}$$

which may be compared to the optimal value of 2.8 radians obtained from equation (33). Then, from figure 5 it is seen that $\Delta V_1 = \Delta V_2 \approx 0.1 V_{c,2}$ or 4.0 kilometers per second, at least. Thus, the total required propulsive effort is about 8.0 kilometers per second or more depending on the value of a . In comparison, the best available multiburn sequence requires 8.6 kilometers per second (using eqs. (32) and (57)) for impulsive thrust, and is more severely penalized for gravity losses since it involves two optimal-angle maneuvers.

The $\sum_1^2 \Delta V$ requirement for the capture - orbit - escape sequence is listed in table I for several values of a . The values of $\sum_1^2 \Delta V$ in the first column were obtained from the present single-burn maneuvers, while the multiburn ΔV 's were obtained by

TABLE I. - PROPULSIVE VELOCITY INCREMENTS

ΔV AT JUPITER

[Hyperbolic velocities, $V_{\infty,1} = V_{\infty,2} = 10$ km/sec;
 angle between hyperbolic asymptotes,
 $\Theta = 4.94$ rad.]

Average vehicle acceleration, $\langle a \rangle$, dimensionless	$\Sigma \Delta V$ for single burn maneuvers, km/sec	$\Sigma \Delta V$ for multiburn maneuvers using Lawden's shift, km/sec
∞	7.92	8.57
0.500	7.92	8.57
.200	7.92	8.58
.100	7.92	8.60
.070	7.92	-----
.050	7.94	-----
.030	7.95	-----
.020	7.96	9.23
.013	8.07	-----
.010	8.35	10.45

combining equation (57) with the optimum-angle results presented in reference 4. It may be noted that the single-burn maneuvers yield ΔV 's that are lower by 0.65 to 2.1 kilometers per second over the range of a that was considered, with the largest reductions at the lowest values of a .

Representative space-vehicle weights (evaluated on arrival at Jupiter's sphere of influence) for these maneuvers are shown in figure 8 as a function of a . Two general types of propulsion systems are considered:

- (1) A solid-core nuclear rocket engine, for which a specific impulse of 900 seconds and engine thrust to Earth weight ratio of 5:1 are reasonable values
- (2) A hypothetical advanced engine (such as a gas-core nuclear rocket), for which a specific impulse of 1800 seconds and a thrust to Earth weight ratio of 1:2 were arbitrarily assumed

For each case it is further assumed that the total payload accelerated away from Jupiter is 100 000 kilograms, that no payload is jettisoned at Jupiter, that the vehicle structure weight is 25 percent of the initial propellant weight, and that a single propulsive stage is used to perform both the capture and escape maneuvers.

Minimum weights clearly occur at relatively low values of dimensionless $\langle a \rangle$, 0.013 and 0.025 for the advanced and solid-core engines, respectively. These values of the mean acceleration a may be translated into initial accelerations a_0 by means of equa-

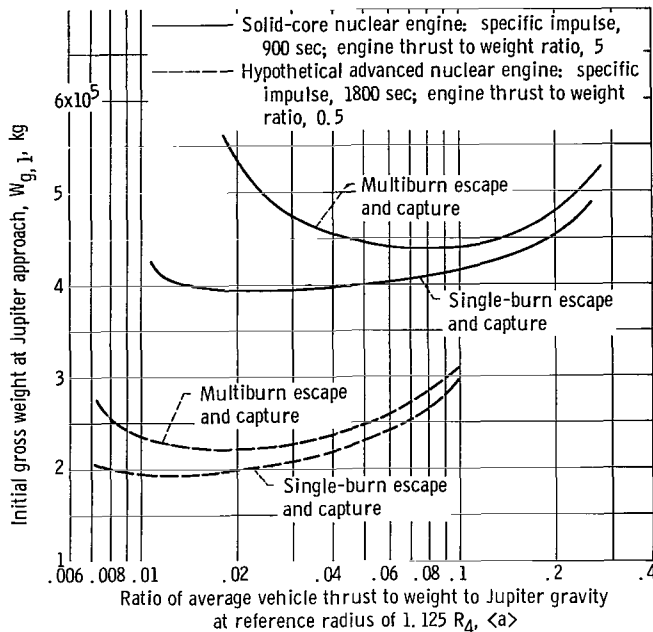


Figure 8. - Selection of desirable thrust to weight ratio for escape and capture maneuvers at Jupiter. Payload, 100 000 kilograms.

tion (3). For the solid-core engine this results in an a_0 of 0.016 local gravity or 0.033 Earth surface gravity. In this case, the most appropriate thrust rating is only 13 000 kilograms or 28 600 pounds. By comparison, an engine four to five times larger would be indicated if the multiburn approach is used; this approach would also involve a total weight penalty of about 45 000 kilograms or 100 000 pounds at Jupiter arrival or about 400 000 pounds in the Earth-centered assembly orbit.¹

These results contrast sharply with those that have been obtained previously in the case of a low circular parking orbit at Earth, where it has generally been found that the most desirable vehicle thrust to weight ratio for a solid-core rocket system is roughly 0.3 local gravity, an order of magnitude higher than the present results suggest. Thus, the optimal utilization of an elliptic orbit produces two effects tending to decrease the desired engine size. First there is the reduction in the optimal thrust to weight ratio that was just pointed out. There is also the basic weight saving for using an elliptic rather than a circular orbit, which (as was illustrated previously in terms of ΔV) can be quite large, especially at the major planets. These effects combined would indicate a reduction in the most advantageous engine size by one or possibly two orders of magnitude.

¹Based on a separate Earth escape stage with the previously mentioned performance parameters and a Δv capability (see ref. 7) of about 8 km/sec.

While it would be improper to base sweeping generalizations on this one example, it has been plainly demonstrated that the present considerations can have a major impact on the question of upper stage engine sizing. A fresh examination of this question, based on the methods described herein, seems to be definitely in order.

CONCLUDING REMARKS

The problem of transferring between specified hyperbolic asymptotes by way of a given planetocentric intermediate orbit has been studied herein. This is a significant problem in space trajectory mechanics which presents itself at the destination planet of an interplanetary round trip. The very important cases where the intermediate orbit is elliptic or hyperbolic have previously been treated only in terms of impulsive thrust; the present work is aimed at optimal-control and finite-thrust aspects of this problem.

The present solutions involve, first, an analysis of minimum effort trajectories for escaping from a highly elliptical (or hyperbolic) orbit and attaining a prescribed asymptotic velocity and direction. Analytical solutions to this subproblem are found for the impulsive and microthrust limits; these provide lower and upper bounds of performance for the general, finite-thrust case which is studied numerically. Second, a simple analytical "matching condition" is derived which, when satisfied jointly by pairs of escape and capture maneuvers, guarantees that the overall capture - orbit - escape sequence is at least locally optimal. Numerical results are then presented (in dimensionless form) for representative cases.

While by no means exhaustive, the present analysis appears to justify several general conclusions which have important implications for future space-mission planning and development.

1. The dramatic ΔV reductions predicted by prior impulsive studies (refs. 5 to 7) for the elliptic parking orbit are maintained and in some cases even enhanced for finite-thrust levels as low as $0.01 \times$ (local gravity). Very-low-thrust systems on the other hand are penalized by large gravity losses. Thus the elliptic parking orbit is most desirable in combination with a medium- to high-thrust propulsion system.

2. For this thrust regime, the gravity losses due to finite thrust and the "steering losses" due to asymptotic direction constraints do not add together directly. That is, the phenomenon of gravity loss is confined to optimal- or near-optimal-angle maneuvers. Heavily constrained trajectories on the other hand involve significant steering losses but there is then little or no additional penalty for finite thrust.

3. In many of the constrained angle cases, the propulsive effort is very insensitive to acceleration. It is shown, however, that the trajectories presented here are actually optimal with respect to thrust control. That is, the thrust switching function, though

numerically small, is never the less significant compared to roundoff error and exhibits the expected type of behavior. The observed insensitivity is easily explained on physical grounds when it is noted that the thrusting maneuver invariably occurs at high altitudes (where the force of gravity is low) if a strong directional constraint is present.

4. Single-burn finite-thrust escape and capture maneuvers appear to be superior to alternative multiburn finite-thrust maneuvers if the asymptotic direction constraint is not excessive. Multiburn solutions yield lower ΔV for severely constrained trajectories, particularly if the asymptotic velocities are high. Further comparisons between the various types of maneuvers will depend on accounting for variations in the heliocentric trajectories, which were assumed fixed for the purposes of this study. It should be noted that the problem studied here is actually a subproblem of the overall trajectory. It would be very desirable to obtain a matching condition to join adjacent heliocentric and planetocentric arcs in a fashion similar to that used herein for joining escape and capture maneuvers.

5. The preceding conclusions imply that it is feasible and probably desirable to employ a small, moderate-thrust engine for the destination-planet maneuvers of future space missions. For instance, the example discussed previously indicates that the optimal thrust to weight ratio for the escape and capture maneuvers of a representative round-trip mission to Jupiter (see fig. 1) would be in the range of 0.02 to 0.06 Earth gravity. Results such as this could open areas of application for types of propulsion systems (such as the gas-core nuclear engine) which might otherwise appear marginal. Moreover, the design trade-offs for engines that are even now being developed could be affected. The present topic should be examined in much greater detail before commitments are made for the development of new types of medium- to high-thrust upper stage propulsion devices.

Lewis Research Center,
National Aeronautics and Space Administration,
Cleveland, Ohio, December 11, 1967,
789-30-01-01-22.

APPENDIX A

SINGULAR ARCS AND PARAMETER OPTIMIZATION

As mentioned previously, the thrust control U_2 is indeterminate if the switching function K is zero over some finite interval. In this case the loss of information occasioned by the failure of equation (15) may, in principle, be overcome by noting that the condition $\mathcal{H} = 0$ now yields two separate relations:

$$\left. \begin{array}{l} F = 0 \\ K = 0 \end{array} \right\} \quad (A1)$$

Since $K = 0$ over a finite interval, the derivatives K' , K'' , ... must also vanish over this interval. Setting $K' = P' = 0$ results in the expression

$$\left(\psi_2 \psi_2' + \frac{\psi_3 \psi_3'}{v^2} - \frac{\psi_3^2 v'}{v^3} \right) = 0 \quad (A2)$$

Using equations (6b), (10b), and (10c) allows equation (A2) to be formally solved for the throttle control U_2 in the form

$$U_{2a} \left[\frac{\sin U_1}{v} \psi_2 - \frac{\psi_3}{v^2} \cos U_1 \right] = X(r, v, \alpha, \psi_1 \dots \psi_4) \quad (A3)$$

Unfortunately, the bracketed term vanishes identically whenever the optimal steering law of equation (13) is used. Although it would be possible to continue in this manner (i. e., by setting $X' = 0$), the resulting expression is so cumbersome as to be completely impractical for either calculation or interpretation. Therefore, an alternate approach is proposed here. Since this report is primarily concerned with the class of single-burn maneuvers, the quantity $U_{2a} = b$ taken together is treated as a design parameter, the constant value of which is to be set before thrusting begins and cannot be changed thereafter. The parameter b is now regarded as a new state variable defined by

$$b' = 0 \quad (A4a)$$

$$b(0) = b(\tau_h), \text{ unconstrained} \quad (A4b)$$

Corresponding to b there is a new adjoint variable ψ_b defined by

$$\psi'_b = -\frac{\partial \mathcal{L}}{\partial b} = 1 - P = -K \quad (\text{A5a})$$

$$\psi_b(0) = \psi_b(\tau_h) = 0 \quad (\text{A5b})$$

where the boundary values (eq. (A5b)) result from application of the transversality condition.

Evidently, equations (A5) are satisfied for any arc that is singular from beginning to end. That is, any constant level of acceleration that produces a singular arc is optimal when viewed as a design parameter.

Equations (A5) are also satisfied in the case of impulsive thrust, since then the burning time is zero. It is also of interest to note that if U_2 were retained as an active control, the conditions for optimal parameter a are

$$a' = 0 \quad (\text{A6a})$$

$$a(0) = a(\tau_h), \text{ unconstrained} \quad (\text{A6b})$$

$$\psi'_a = U_2(1 - P) \quad (\text{A7a})$$

$$\psi_a(0) = \psi_a(\tau_h) = 0 \quad (\text{A7b})$$

In this case, the quantity $U_2(1 - P)$ is nonpositive (since $U_2 = 0$ if $P = 1$) and hence,

$$\psi_a(\tau_h) \leq 0 \quad (\text{A8})$$

provided that $\psi_a(0) = 0$. Thus, if unlimited throttling control is admitted, the only possible form of optimal trajectory in the present context consists of either impulses or singular arcs in combination with coasting (zero thrust) arcs. That is, no finite-thrust level can be optimal except as it occurs in a singular arc.

In other cases, finite acceleration produces a negative value of $\psi_a(\tau_h)$ which implies that Δv could have been reduced by raising a . This is a general conclusion and is not limited to the present problem which after all is distinguished from other space trajectory problems (such as orbit transfer) only by the form of the boundary and transversality conditions.

APPENDIX B

PARTIAL DERIVATIVES FOR THE TRANSVERSALITY CONDITIONS

The transversality condition at τ_o requires that

$$\vec{\psi}_o \cdot \vec{T}_o = 0 \quad (B1)$$

where \vec{T}_o is the tangent vector to the inner manifold which is defined (after substituting eq. (7a) into eqs. (7b) to (7e)) by the following relations:

$$\left. \begin{aligned} r_o &= \frac{1 + e_{po}}{1 + e_{po} \cos \nu_{po}} & \theta_o &= \nu_{po} \\ v_o &= \left(\frac{2 + 2e_{po} \cos \nu_{po}}{1 + e_{po}} - 1 + e_{po} \right)^{1/2} & \Delta v_o &= 0 \\ \tan \alpha_o &= \frac{e_{po} \sin \nu_{po}}{1 + e_{po} \cos \nu_{po}} \end{aligned} \right\} \quad (B2)$$

Now the components of \vec{T}_o are

$$\left(\frac{\partial r_o}{\partial \nu_{po}}, \frac{\partial v_o}{\partial \nu_{po}}, \frac{\partial \alpha_o}{\partial \nu_{po}}, \frac{\partial \theta_o}{\partial \nu_{po}}, 0 \right) \quad (B3)$$

Carrying out the indicated differentiations gives equation (B1) in the form

$$\begin{aligned} \psi_{10} \frac{r_o^2}{1 + e_{po}} (e_{po} \sin \nu_{po}) + \psi_{20} \left[\frac{-1}{v_o (1 + e_{po})} \right] (e_{po} \sin \nu_{po}) \\ + \psi_{30} \left[\frac{e_{po} r_o^2 \cos^2 \alpha_o}{(1 + e_{po})^2} (\cos \nu_{po} + e_{po}) \right] + \psi_4 = 0 \end{aligned} \quad (B4)$$

which may be written after simplification as

$$\sin \nu_{po} = \frac{-1}{\psi_{10} r_o^2 - \frac{\psi_{20}}{v_o}} \left[\psi_{30} r_o^2 \cos^2 \alpha_o \left(\frac{\cos \nu_{po} + e_{po}}{1 + e_{po}} \right) + \frac{1 + e_{po}}{e_{po}} \psi_4 \right] \quad (\text{B5})$$

At time τ_h , the hyperbolic manifold is defined using v and α as surface coordinates:

$$\left. \begin{aligned} r &= r(v) \\ v &= v \\ \alpha &= \alpha \\ \theta &= \theta(v, \alpha) \end{aligned} \right\} \quad (\text{B6})$$

In this case the transversality condition requires that

$$\left. \begin{aligned} \vec{\psi}_h \cdot \vec{T}_{1h} &= 0 \\ \vec{\psi}_h \cdot \vec{T}_{2h} &= 0 \end{aligned} \right\} \quad (\text{B7})$$

where the two tangent vectors are

$$\left. \begin{aligned} \vec{T}_{1h} &= \left(\frac{\partial r}{\partial v}, 1, 0, \frac{\partial \theta}{\partial v} \right) \\ \vec{T}_{2h} &= \left(0, 0, 1, \frac{\partial \theta}{\partial \alpha} \right) \end{aligned} \right\} \quad (\text{B8})$$

Now from equation (8a),

$$r_h = \frac{2}{v_h^2 - v_\infty^2}$$

hence,

$$\left. \frac{\partial \mathbf{r}}{\partial \mathbf{v}} \right|_{\mathbf{h}} = -\mathbf{r}_{\mathbf{h}}^2 \mathbf{v}_{\mathbf{h}} \quad (\text{B9})$$

Also, from equation (8c)

$$\theta_{\mathbf{h}} = \theta_{\infty} + \varphi_{\mathbf{h}} - \varphi_{\infty}$$

Then differentiating equations (8e) and (8f) with respect to $\mathbf{v}_{\mathbf{h}}$ and $\alpha_{\mathbf{h}}$

$$\left. \begin{aligned} \frac{\partial \theta_{\mathbf{h}}}{\partial \mathbf{v}_{\mathbf{h}}} &= \frac{\partial \varphi_{\mathbf{h}}}{\partial \mathbf{v}_{\mathbf{h}}} - \frac{\partial \varphi_{\infty}}{\partial \mathbf{v}_{\mathbf{h}}} \\ \frac{\partial \theta_{\mathbf{h}}}{\partial \alpha_{\mathbf{h}}} &= \frac{\partial \varphi_{\mathbf{h}}}{\partial \alpha_{\mathbf{h}}} - \frac{\partial \varphi_{\infty}}{\partial \alpha_{\mathbf{h}}} \end{aligned} \right\} \quad (\text{B10})$$

where

$$\left. \begin{aligned} \frac{\partial \varphi_{\mathbf{h}}}{\partial \mathbf{v}_{\mathbf{h}}} &= \frac{\sin^2 \varphi_{\mathbf{h}}}{\sin \alpha_{\mathbf{h}} \cos \alpha_{\mathbf{h}}} \left(\frac{\mathbf{v}_{\infty}^2}{\mathbf{v}_{\mathbf{h}}^3} \right) \\ \frac{\partial \varphi_{\mathbf{h}}}{\partial \alpha_{\mathbf{h}}} &= \sin^2 \varphi_{\mathbf{h}} \left[\cot \varphi_{\mathbf{h}} (\cot \alpha_{\mathbf{h}} - \tan \alpha_{\mathbf{h}}) + 2 \right] \\ \frac{\partial \varphi_{\infty}}{\partial \mathbf{v}_{\mathbf{h}}} &= \frac{\sin^2 \varphi_{\infty}}{2 \cos \alpha_{\mathbf{h}}} \left(\frac{\mathbf{v}_{\infty}}{\mathbf{v}_{\mathbf{h}}^2} + \frac{1}{\mathbf{v}_{\infty}} \right) \\ \frac{\partial \varphi_{\infty}}{\partial \alpha_{\mathbf{h}}} &= -\sin \varphi_{\infty} \cos \varphi_{\infty} \tan \alpha_{\mathbf{h}} \end{aligned} \right\} \quad (\text{B11})$$

These are the relations needed for the evaluation of equations (17) and (18).

APPENDIX C

NEAR-OPTIMAL FEEDBACK SOLUTION

The previously described technique of solution, consisting of a numerical search to zero the variational "terminal error function" (see eq. (46)), is quite appropriate for the purposes discussed in the text because it precisely defines the minimal Δv and other features of the optimal trajectories. Unfortunately, it requires extensive computational effort, and there are numerous cases in which a less precise but faster and more flexible technique of solution would be more suitable.

One such technique is presented in this appendix. A suboptimal but strongly convergent feedback algorithm is used to compute the steering signal $U_1(\tau)$. This provides a feasible solution of the two-point boundary value problem in every case. That is, the desired terminal values are always attained (though not for minimum Δv) in spite of initial-condition errors or other disturbances. Optimality is approached by introducing an arbitrary power series into the feedback loop to temporarily bias the aiming data (θ_∞) fed into the steering algorithm. The coefficients of the series are then determined by direct numerical search to yield minimum Δv . Thus, the variational two-point boundary value problem is eliminated in favor of a more tractable and conceptually simpler problem in the ordinary calculus. As will be seen, the "true" (i. e., variational) minimum Δv can be attained within practical tolerances by considering only the first few terms of the biasing series.

A Basic Feedback Algorithm

To eliminate the difficulties of the two-point boundary value problem, an alternative scheme must necessarily rely on the inherent goal-seeking nature of feedback control. The impulsive solution described previously does in fact possess the necessary closed-loop or goal-seeking character. That is, the proper angle of attack may be found by means of equations (19) to (25) as a function of the current values of the state variables (r , v , α , and θ) and of the desired terminal conditions (v_∞ and θ_∞).

This scheme may be extended immediately to the case of finite thrust. At every instant, the "velocity to gain" vector Δv_g whose components are given by equations (24) and (25) is computed just as though the remainder of the trajectory were to be performed impulsively. Although Δv_g must now be computed repeatedly during the maneuver, each calculation requires no information beyond the current state variables and the desired terminal conditions. This is, in fact, a feedback control policy for the stated problem; the computational algorithm is given by equations (19) to (25) with r_h , v_o , α_{po} , and ν_{po}

replaced by the current values of the state variables $r(\tau)$, $v(\tau)$, $\alpha(\tau)$, and $\theta(\tau)$.

This is sometimes referred to as the "cross-product" rule, because (in 3 dimensions) the alinement of \vec{a} and $\Delta\vec{v}_g$ corresponds to the condition

$$\vec{a} \times \Delta\vec{v}_g = \vec{0} \quad (C1)$$

As was shown in the ANALYSIS, this policy is actually optimal in the impulsive limit; it is also known to be fairly efficient for high-thrust systems such as chemical rockets (see ref. 13). Moreover, it produces the largest possible instantaneous rate of decrease of Δv_g , regardless of the acceleration level. This is easily seen by taking the time derivative of equation (24):

$$\Delta v_g (\Delta v_g)' = v_h' (v_h - v \cos \beta) + v' (v - v_h \cos \beta) + v v_h \sin \beta (\alpha_h' - \alpha') \quad (C2)$$

In equation (6), it is noted that only v' and α' depend explicitly on U_1 . Thus,

$$\frac{\partial \Delta v_g'}{\partial U_1} = 0 = \frac{\partial v'}{\partial U_1} (v - v_h \cos \beta) - \frac{\partial \alpha'}{\partial U_1} (v v_h \sin \beta)$$

or

$$\frac{\frac{\partial v'}{\partial U_1}}{\frac{\partial \alpha'}{\partial U_1}} = \frac{v v_h \sin \beta}{v - v_h \cos \beta} = \frac{-a \sin U_1}{\frac{a \cos U_1}{v}} = -v \tan U_1$$

Hence,

$$\tan U_1 \Big|_{\max \Delta v_g'} = \frac{v_h \sin \beta}{v_h \cos \beta - v} \quad (C3)$$

That this represents a maximum rate of decrease is seen by noting that

$$\frac{\partial^2 \Delta v_g'}{\partial U_1^2} = a \cos U_1 \left[(v_h \cos \beta - v) + \frac{v_h^2 \sin^2 \beta}{v_h \cos \beta - v} \right] \quad (C4)$$

Since $v_h \geq v$, $\cos U_1$ and the quantity $v_h \cos \beta - v$ has the same sign.

Convergence and Stability

For the same reason, the convergence of this algorithm is assured for sufficiently high thrust. In that case, equation (C2) is dominated by the terms

$$a \cos U_1 (v - v_h \cos \beta) - v v_h \sin \beta \left(\frac{a \sin U_1}{v} \right) \quad (C5)$$

and Δv_g approaches zero monotonically. Even when the terms in equation (C5) are not clearly dominant, it appears that convergence can be attained without difficulty as long as the steering signal remains within the first or fourth quadrants. That is, it was shown in the Mean value solution section (p. 20) that the instantaneous rate of adding energy per unit mass is

$$\left[\frac{1}{2} v_\infty^2(\tau) \right]' = a v \cos U_1 \quad (C6)$$

and hence $v_\infty^2(\tau)$ increases monotonically toward its desired value so long as $\cos U_1$ is positive (U_1 in quadrant 1 or 4). After local escape energy ($v_\infty^2 = 0$) has been attained in this manner, the vehicle must necessarily begin to traverse an arc along which r increases monotonically, which implies that $r' > 0$. From equation (8a) it is recalled that

$$v_h^2(\tau) = v_{\infty, des}^2 + \frac{2}{r(\tau)} \quad (C7)$$

so that

$$v_h' = \frac{-r'}{r^2 v_h} \quad (C8)$$

Hence, when r' is positive and U_1 is in quadrant 1 or 4, the velocity to gain Δv_g approaches zero monotonically regardless of thrust level, because every term in equation (C2) is then negative. (Actually, it is clear that these conditions need only be satisfied over the terminal portion of the trajectory to guarantee convergence.) As a point of interest, it is clear from the preceding discussion that $(\Delta v_g)^2$ may serve as a Lyapounov

stability function for this problem (see ref. 14). That is, a region of asymptotic stability exists for sufficiently large r , and this region is attainable by every steering control which lies entirely in the first and/or fourth quadrants.

Optimal Compensation

Although the preceding "cross-product" algorithm is optimal only in the limit of very high (impulsive) thrust, its strong convergence properties suggest that it would also be useful for the medium-thrust regime of interest here. Unfortunately, initial numerical simulations proved disappointing. Although the stated convergence properties were clearly demonstrated, a serious reduction in propulsive efficiency was noted for accelerations lower than about 0.2 local gravity. The reason for this is not hard to find and can easily be understood by considering figure 9. There, three impulsive trajectories are illustrated which depart from different points on an ellipse and attain the optimal value of θ_∞ defined by equation (33). As has been previously noted, the minimum energy trajectory departs from periapse (position 1) and employs tangential steering, $U_1 = 0$. If the impulse occurs before periapse (position 2) a sizable negative angle of attack is required to produce a trajectory that will attain the necessary value of θ_∞ . Similarly, a late impulse (point 3) requires a positive angle of attack. Now it was shown in reference 4 that a finite-thrust arc is generally "centered" on the location of the equivalent impulse. This means that for an optimal-angle trajectory, the powered arc is distributed into roughly

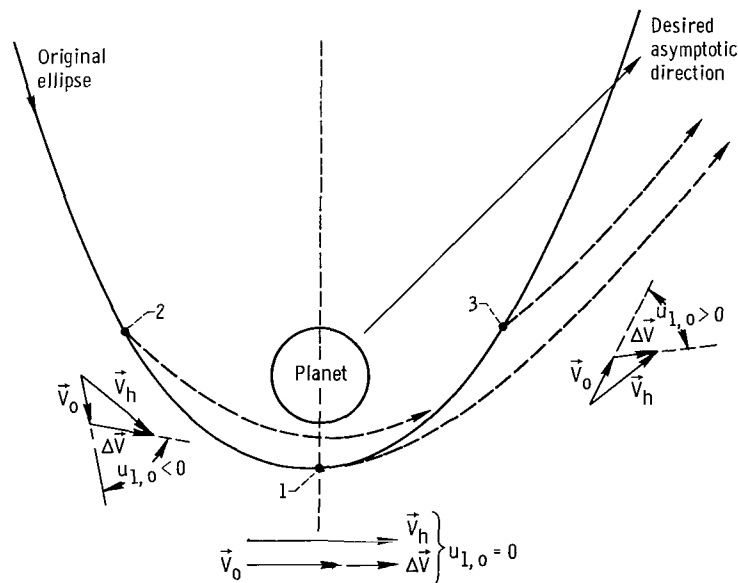


Figure 9. - Impulsive trajectories attaining the same asymptotic direction.

equal central angles ahead of and behind the original periapse. For vehicle accelerations of the order of 0.01 local gravity the "lead angle" ν_{po} is of the order of -1 to -2 radians. Thus, initially the elementary controller would command a large negative angle of attack (≈ -1.4 rad); the commanded value would gradually approach zero as the original periapse position is approached and finally increase to a sizable positive value. In view of equation (38), this behavior, illustrated in figure 10(a) for $a = 0.02$, leads to a large increase in Δv .

On the other hand, the preceding algorithm (eqs. (19) to (25)) can be inverted to compute instantaneous values of θ_∞ along an arbitrary trajectory. When this procedure is applied to the optimal-angle trajectories presented in reference 4, it is found that, in the thrust regime of interest, the optimal value of θ_∞ is initially biased by -0.1 to -0.4

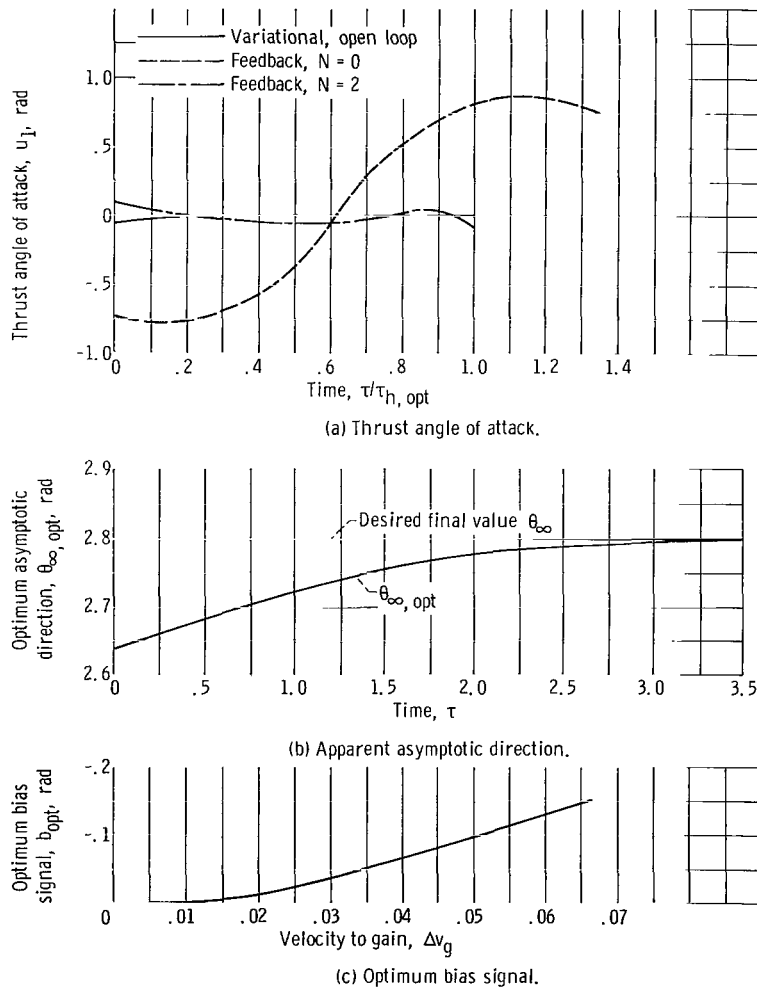


Figure 10. - Comparison of control histories. Dimensionless acceleration, $a = 0.02$; parking orbit eccentricity, $e_{pp} = 0.9$; asymptotic central angle, $\theta_\infty = 2.8$ radians; hyperbolic excess velocity, $v_\infty = 0.25$.

radians and increases asymptotically toward the desired value. A typical example is illustrated in figure 10(b), where $\theta_{\infty, \text{opt}}$ is plotted against τ for an optimal trajectory with $e_{\text{po}} = 0.9$, $a = 0.02$, $v_{\infty} = 0.25$, and $\theta_{\infty, \text{des}} = 2.8$ radians. The bias signal

$$b = \theta_{\infty, \text{des}} - \theta_{\infty, \text{opt}} \quad (\text{C9})$$

is plotted against Δv_g in figure 10(c). It is clear from this that the optimal bias signal can be represented in the form

$$b_{\text{opt}}(\tau) = \sum_{n=1}^{\infty} b_n Y^n \quad (\text{C10})$$

where

$$Y = \frac{\Delta v_g(\tau)}{\Delta v_g(0)}$$

and can in fact be rather well approximated by keeping only the first few terms of this series. Equation (C10) is used as the basis of a compensator. This modifies the θ_{∞} signal fed into the cross product algorithm, equations (19) to (25), in such a way as to produce a value of $U_1(\tau)$ which, in the absence of perturbations, is very nearly the same as $U_1(\tau)_{\text{opt}}$. That is,

$$\theta_{\infty}(\tau) = \theta_{\infty, \text{des}} + b_{\text{opt}}(\tau) \quad (\text{C11})$$

where b_{opt} is defined by equation (C10). It is postulated that optimal values of the b_i , determined in a nominal unperturbed case by the Ritz method of numerical optimization (see ref. 15), will remain very nearly optimal when a small trajectory perturbation is introduced. Example perturbations include (1) errors in initial conditions, (2) off-nominal engine performance, and (3) errors in the form of the state equations (eqs. (6)). The present, compensated cross-product algorithm is shown to be capable of withstanding rather large perturbations of these kinds without violating the desired boundary values ($v_{\infty, \text{des}}$ and $\theta_{\infty, \text{des}}$) and with only a small penalty as compared to the variational solution in which the same perturbation is accounted for.

Comparison of Open-Loop and Closed-Loop Results

The first question to be discussed is whether, or how fast, the Ritz compensated cross-product algorithm can be made to approach the corresponding open-loop optimal results presented in the text. Toward this end, consider again the optimal-angle escape problem for $e_{po} = 0.9$ and $v_{\infty} = 0.25$. (By eq. (33), the value of $\theta_{\infty, opt} = 2.8$ rad.) In figure 11, the Δv penalty for using the present controller rather than open-loop varia-

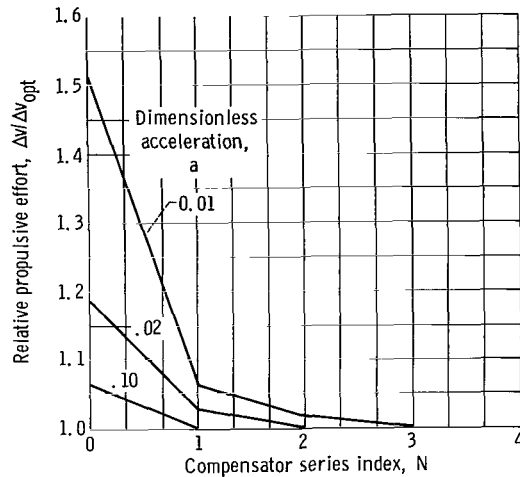


Figure 11. - Effect of truncating compensator series. Parking orbit eccentricity, $e_{po} = 0.9$; asymptotic central angle, $\theta_{\infty} = 2.8$ radians; hyperbolic excess velocity, $v_{\infty} = 0.25$.

tional steering is presented as a function of N , the index of the compensator series. Values of a of 0.1, 0.02, and 0.01 local gravity are represented by the lower, middle, and upper curves, respectively. For relatively high acceleration, the Δv penalty is small even at $N = 0$, and for practical purposes it is eliminated by including one term in the series. For $a = 0.02$, the initial penalty is larger and two terms are needed to sensibly eliminate it. (Its control history was compared with that for $N = 0$ and variational steering in fig. 10.) The case where $a = 0.01$ is considerably more difficult, requiring at least $N = 3$ to bring the penalty down to an acceptable level.

From these observations, the following are immediately inferred:

- (1) For a given value of N , the penalty decreases rapidly as a increases. (Recall that the uncompensated policy was shown to be optimal for impulsive thrust.)
- (2) For a given value of a , the Δv penalty is reduced by nearly an order of magnitude when N is increased by one unit.
- (3) In the absence of perturbations, the variational Δv can be approached within ar-

bitrary tolerances by choosing a large enough value of N , if the coefficients $b_1 \dots b_N$ are selected optimally.

Some very desirable properties of the compensated policy were demonstrated previously for the case where θ_∞ is not constrained. These advantages also remain in full force when angular constraints are imposed (i. e., values of θ_∞ different from that given by eq. (33)). Refer again to figure 5 where values of the propulsive Δv , normalized by equation (32), are plotted as functions of θ_∞ for the entire range $0 \leq \theta_\infty \leq 2\pi$. The lower, solid curves represent the optimal impulsive solution discussed previously; the others represent various finite values of a . For fixed values of a as low as 0.01, the present closed-loop controller yields Δv 's which are virtually as low as those obtained by variational means. That is, with the compensator series $N \leq 3$, the Δv penalties are not discernible to the scale of figure 5.

It may also be recalled that, for $a \geq 0.01$, the low-thrust trajectories are virtually as efficient as the impulsive ones except in the immediate vicinity of $\theta_{\infty, \text{opt}}$. In the nonoptimal-angle region, the results are quite insensitive to the acceleration level, so much so that 0.01 local "g" behaves almost like an impulse. In this insensitive region, the Δv 's resulting from the present controller approach the variational minimum even more rapidly than in the optimal-angle case. For example, when $a = 0.01$ and $\theta_\infty = 3.34$ radians, the variational Δv was approached within 0.3 percent by using only one term in the compensator series. (For the optimal-angle case, three terms had to be used in achieve a comparable result.) In this sense the present scheme appears even more advantageous in the nonoptimal-angle region than it did for optimal-angle trajectories.

The two trajectories just cited are the ones that were illustrated geometrically in figure 6. Figure 6(a) represents the optimal-angle case with $\theta_\infty = 2.8$, and figure 6(b) covers the trajectory where $\theta_\infty = 3.34$. Recall that r, v, α , and the control variables are plotted as functions of the central angle θ . Solid and dashed lines represent the variational open-loop results, and dotted lines denote the closed-loop results with $N = 2$. In either case, the only difference discernible to the scale of figure 6 is in the steering control history U_1 . As has been previously noted, the present control action oscillates slowly about the variational control history. In the optimal-angle case, the oscillations occur around a near-zero nominal value and hence produce a definite second-order effect on $\langle v \cos U_1 \rangle$. For the constrained case, the oscillations take place around a strong nominal steering action; the effect is hence to increase $\cos U_1$ in one place and decrease it in another. As a net result there is a cancellation effect, and the change in $\langle v \cos U_1 \rangle$ is considerably smaller than second order.

Effect of Perturbations

The previous results confirm the analytical predictions that were made about the efficiency of the Ritz-compensated cross-product algorithm. It finally remains to demonstrate its closed-loop aspect - that is, its ability to attain the prescribed boundary conditions in spite of perturbations (such as a poor choice of initial search variables) which would cause the open-loop variational procedure to diverge. Toward this end, the nominal trajectory depicted in figure 6(a) (optimal-angle case) was subjected to sizable variations in the initial conditions and in the acceleration level a . The results are compared with corresponding variational runs in table II. For both schemes, the propulsive Δv

TABLE II. - EFFECT OF TRAJECTORY PERTURBATIONS ON GRAVITY AND
STEERING LOSS PROPULSIVE VELOCITY INCREMENT

CORRECTION FACTOR f_v

[Parking orbit eccentricity, $e_{po} = 0.9$; dimensionless hyperbolic velocity, $v_\infty = 0.25$;
asymptotic direction, $\theta_\infty = 2.80$ rad; dimensionless acceleration, $a = 0.02$.]

Perturbation	Present results (for N = 2; constant b_1 and b_2)	Variational results (reiterated)	Difference, percent
None	1.1391	1.1373	0.16
Initial true anomaly, $\nu_{po}: 6^\circ$	1.1764	1.1690	.63
Initial true anomaly, $\nu_{po}: -6^\circ$	1.1589	1.1504	.74
Dimensionless acceleration, $a: -10$ percent	1.1911	1.1842	.58

(normalized by eq. (32)) is presented for the nominal case and with perturbations of $\pm 6^\circ$ on the initial position ν_{po} and -10 percent on the acceleration level. In all cases, the present algorithm, using the same values of b_1 and b_2 determined for the nominal case, had no difficulty in attaining the required boundary values, and involved only fractional percentage penalties in Δv as compared to the reiterated variational trajectories. As was pointed out previously, reiteration is required in the variational case to recover the desired boundary values; this implies a priori knowledge of the perturbation. It was noted that the Δv difference between the present and variational results could be reduced to 0.16 percent or less in the perturbed cases by reoptimizing b_1 and b_2 ; this also assumes a priori knowledge of the perturbation and is perhaps a more representative comparison than that indicated in table II.

REFERENCES

1. Lawden, Derek F.: *Optimal Trajectories for Space Navigation*. Butterworth and Company, 1963.
2. Moeckel, W. E.: *Trajectories with Constant Tangential Thrust in Central Gravitational Fields*. NASA TR R-53, 1959.
3. Lebedev, V. N.: *Variational Problem of Escape from Circular Orbit*. Rep. No. FTD-TT-64-1200/1+2+4, Foreign Technology Div., Air Force Systems Command, Dec. 5, 1964. (Available from DDC as AD-610208.)
4. Willis, Edward A., Jr.: *Finite-Thrust Escape from and Capture Into Circular and Elliptic Orbits*. NASA TN D-3606, 1966.
5. Luidens, Roger W.; and Miller, Brent A.: *Efficient Planetary Parking Orbits with Examples for Mars*. NASA TN D-3220, 1966.
6. London, Howard S.: *Escape from Elliptical Parking Orbits*. Paper No. 66-127, American Astronautical Society, July 1966.
7. Luidens, Roger W.; Miller, Brent A.; and Kappraff, Jay M.: *Jupiter High-Thrust Round-Trip Trajectories*. NASA TN D-3739, 1966.
8. Gobetz, Frank W.: *Optimum Transfers Between Hyperbolic Asymptotes*. AIAA J., vol. 1, no. 9, Sept. 1963, pp. 2034-2041.
9. Edelbaum, T. N.: *How Many Impulses?* Paper No. 66-7, AIAA, Jan. 1966.
10. Pontriagin, Lev S., et al., (K. N. Trirgoff, trans.): *The Mathematical Theory of Optimal Processes*. Interscience Publishers, 1962.
11. Ehrlicke, Krafft A.: *Principles of Guided Missile Design*. Vol. 1 of Space Flight. D. Van Nostrand Co., Inc., 1960, pp. 332-334.
12. Powell, M. J. D.: *An Efficient Method for Finding the Minimum of a Function of Several Variables without Calculating Derivatives*. Computer J., vol. 7, no. 2, July 1964, pp. 155-162.
13. Battin, Richard H.: *Astronautical Guidance*. McGraw-Hill Book Co., Inc., 1964.
14. Hahn, Wolfgang (Hans H. Hosenthien and Siegfried H. Lehnigk, trans.): *Theory and Application of Liapunov's Direct Method*. Prentice-Hall, Inc., 1963.
15. Kantorovich, Leonid V.; and Krylov, V. I. (Curtis D. Benster, trans.): *Approximate Methods of Higher Analysis*. Second ed., John Wiley and Sons, Inc., 1962, pp. 258-269.

FIRST CLASS MAIL

110 001 53 51 305 68106 00903
AIR FORCE WEAPONS LABORATORY/AFWL/
KIRTLAND AIR FORCE BASE, N. MEXICO 8711

POSTMASTER: If Undeliverable (Section 158
Postal Manual) Do Not Return

POSTMASTER: If Undeliverable (Section 158
Postal Manual) Do Not Return

"The aeronautical and space activities of the United States shall be conducted so as to contribute . . . to the expansion of human knowledge of phenomena in the atmosphere and space. The Administration shall provide for the widest practicable and appropriate dissemination of information concerning its activities and the results thereof."

—NATIONAL AERONAUTICS AND SPACE ACT OF 1958

NASA SCIENTIFIC AND TECHNICAL PUBLICATIONS

TECHNICAL REPORTS: Scientific and technical information considered important, complete, and a lasting contribution to existing knowledge.

TECHNICAL NOTES: Information less broad in scope but nevertheless of importance as a contribution to existing knowledge.

TECHNICAL MEMORANDUMS: Information receiving limited distribution because of preliminary data, security classification, or other reasons.

CONTRACTOR REPORTS: Scientific and technical information generated under a NASA contract or grant and considered an important contribution to existing knowledge.

TECHNICAL TRANSLATIONS: Information published in a foreign language considered to merit NASA distribution in English.

SPECIAL PUBLICATIONS: Information derived from or of value to NASA activities. Publications include conference proceedings, monographs, data compilations, handbooks, sourcebooks, and special bibliographies.

TECHNOLOGY UTILIZATION PUBLICATIONS: Information on technology used by NASA that may be of particular interest in commercial and other non-aerospace applications. Publications include Tech Briefs, Technology Utilization Reports and Notes, and Technology Surveys.

Details on the availability of these publications may be obtained from:

**SCIENTIFIC AND TECHNICAL INFORMATION DIVISION
NATIONAL AERONAUTICS AND SPACE ADMINISTRATION
Washington, D.C. 20546**